Effects of Multi-walled Carbon Nanotubes (MWCNTs) and integrated MWCNTs/SiO_2 Additives on Polymeric PVDF Membrane for Membrane Distillation

Rufan Zhou

Thesis submitted to the University of Ottawa

in partial Fulfillment of the requirements for the

Master of Applied Science in Chemical Engineering

Department of Chemical and Biological Engineering

uOttawa

University of Ottawa

Abstract

Multi-walled carbon nanotubes (MWCNTs) and integrated MWCNTs/ SiO_2 nanoparticles (NPs) were loaded as additives into nanocomposite polyvinylidene fluoride (PVDF) membranes fabricated via phase inversion methods, and the effects of these additives on the structure and vacuum membrane distillation (VMD) performance of the membranes have been studied. With an appropriate amount of MWCNTs (2 wt.% to PVDF) blended into the membrane, VMD performance of membrane was improved significantly due to higher membrane porosity, contact angle and surface roughness without extreme compromise of liquid entry pressure of water (LEPw), which could reach up to 72 psi. Further integration of MWCNTs with a small amount of SiO_2 nanoparticles (NPs) showed a synergic effect resulting in further improvement of VMD flux due primarily to the increase in surface pore size. When the amount of SiO_2 NPs additive was large, the effects of NPs dominates the VMD performance. However, the asymmetric structure of PVDF membrane disappears, which exercises an unfavorable effect on VMD performance. All fabricated membranes exhibited a great desalination potential with extremely high salt rejection (>99.98%). The incorporation of MWCNTs did not improve the tensile properties of the membrane.

Abstrait

Des nanotubes de carbone à parois multiples (MWCNT) et des nanoparticules (NP) MWCNT/SiO_2 intégrées ont été chargés comme additifs dans des membranes de polyfluorure de vinylidène (PVDF) nanocomposites fabriquées par des méthodes d'inversion de phase, et les effets de ces additifs sur la performance de la structure et de la distillation membranaire sous vide (VMD) des membranes ont été étudiés. Avec une quantité appropriée de MWCNT mélangés dans la membrane (2% en poids de PVDF), la performance VMD de la membrane a été améliorée de manière significative en raison de la porosité de la membrane, de l'angle de contact et de la rugosité de surface plus élevés sans compromis extrême avec une pression (LEPw) d'eau liquide pouvant atteindre 72 psi. Une intégration plus poussée des MWCNT avec une petite quantité de nanoparticules de SiO_2 (NP) a montré un effet synergique résultant en une amélioration supplémentaire du flux de VMD dû principalement à l'augmentation de la taille des pores de surface. Lorsque la quantité d'additif de NP SiO_2 était importante, les effets des NP dominent la performance VMD. Cependant, la structure asymétrique de la membrane PVDF disparaît, ce qui exerce un effet défavorable sur les performances du VMD. Toutes les membranes fabriquées présentaient un excellent potentiel de dessalement avec un rejet de sel extrêmement élevé (> 99.98%). L'incorporation de MWCNT n'a pas amélioré les propriétés de traction de la membrane.

Acknowledge

I would like to express my sincere appreciation to my supervisor and co-supervisor Dr. Christopher Lan and Dr. Takeshi Matsuura for the opportunity, their guidance and supports. Special thanks to and Dr. Dipak Rana for his hands-on guidance and help. All your efforts and dedication are priceless and greatly appreciated.

My gratitude also goes to the administrative and technical staff in the Department of Chemical and Biological Engineering, Faculty of Engineering at the University of Ottawa, especially to Sylvie Saindon, Francine Pétrin, James Macdermid and Franco Ziroldo for their valuable help in administrative and technical affairs.

I would also like to acknowledge the Centre for Catalysis Research and Innovation in our university through Dr. Yun Liu for her tremendous support with SEM analysis and the Centre for Research in Photonics for their precious support with AFM tests.

Special gratitude to all the members of our membrane research group especially Mohammadali Baghbanzadeh, Johnson E. Efome, Viyash Murugesan and Zhelun Li for their inspirational support and help to me all through the course of this work.

Finally, I am grateful to my beloved parents and lovely girlfriend for their love, support and encouragement in my life.

Table of Contents

Abstract ..... **II**

Abstrait ..... **III**

Acknowledge ..... **IV**

Table of Contents ..... **V**

List of Figures ..... **VIII**

List of tables ..... **X**

Nomenclature ..... **XI**

Abbreviations ..... **XII**

1. Introduction **1**

Reference 4

2. Literature review **7**

2.1. Membrane distillation (MD) 8

2.1.1. Membrane distillation configurations 8

2.1.2. Configurations of MD modules 12

2.1.3. Membranes for MD 14

2.2. Carbon nanotubes and their application into MD. 18

2.2.1. Characteristics of Carbon nanotubes 18

2.2.2. CNTs application on MD 19

2.2.3. Comparison of CNTs with other inorganic additives. 21

Reference 23

3. Effects of multi-walled carbon nanotubes on PVDF nanocomposite membranes for vacuum membrane distillation **33**

Statement of manuscript status and author contribution 33

Highlights 34
Graphical abstract 34
Abstract 34
Key words 35
3.1. Introduction 35
3.2. Experiment 38
3.2.1. Materials 38
3.2.2. Membrane fabrication 39
3.2.3. Membrane characterization 40
3.2.4. Liquid entry pressure of water (LEPw) measurement 41
3.2.5. Vacuum membrane distillation (VMD) 42
3.3. Results and discussion 43
3.3.1. The effects of MWCNTS on the top surface morphology 43
3.3.2. Effects of MWCNTs on cross-sectional structure of membrane 45
3.3.3. Tensile property of MWCNTs blended membranes 50
3.3.4. The VMD performances and LEPw of MWCNTs blended membrane 51
3.3.5. Related researches focusing on CNTs application for desalination by MD 54
3.4. Conclusions 57
Reference 57
4. Hybrid SiO_2/multi-walled carbon nanotubes (MWCNTs) nanocomposite PVDF membranes for vacuum membrane distillation 66
Highlights 66
Graphical abstract 67
Abstract 67

Key words 68
4.1. Introduction 68
4.2. Experiment 70
4.2.1. Materials 70
4.2.2. Membrane fabrication 71
4.2.3. Membrane characterization 72
4.2.4. Particles characterization and aggregation analysis 74
4.2.5. Liquid entry pressure of water (LEPw) measurement 74
4.2.6. Vacuum membrane distillation (VMD) 75
4.3. Results and discussion 77
4.3.1. Hybrid nanocomposite membranes with low SiO_2 NPs content (1%) 77
4.3.2. Hybrid nanocomposite membranes with high SiO_2 NPs content (7 %) 84
4.3.3. The effect of SiO_2 NPs addition on the aggregate size 88
4.4. Conclusions 92
Reference 93
5. Conclusions 100

List of Figures

Fig. 2-1 Schematic principles of vapor transport in MD process[15]. 9

Fig. 2-2 Schematic diagram of four basic MD configuration[8]. 10

Fig. 2-3 Schematic of three typical MD modules[8]. 13

Fig. 2-4 Typical cross-sectional SEM pictures of membrane 17

Fig. 2-5 Mechanisms of MD in the presence of CNTs[77]. 20

Fig. 2-6 Effect of increased roughness on vapor transport in the CNTs membranes[46]. 21

Fig. 3-1 Graphical abstract of MWCNTs effects on membrane.....34

Fig. 3-2 SEM images of the top surface of membranes with different MWCNTs loading loadings.....44

Fig. 3-3 Top surface of membranes with different MWCNTs loadings 44

Fig. 3-4 SEM image of cross-sectional area on membranes with different MWCNTs loading ratio. 45

Fig. 3-5 SEM image of different cross-sectional areas on membranes.. 47

Fig. 3-6 VMD performances and LEPw of membrane with different concentration of MWCNTs 52

Fig. 3-7 Flux and rejection performance of membrane for long-term operation 53

Fig. 3-8 Flux and rejection performance of membrane for different feed side temperature 53

Fig. 3-9 Possible CNT's impacts on membrane structure and vapor permeation 54

Fig. 4-1 Possible mechanism of integrated additives loaded on membrane.....67

Fig. 4-2 Schematic illustration of VMD setup[25].....76

Fig. 4-3 SEM image of top surface of membranes listed in Table 4-2. 79

Fig. 4-4 SEM cross-sectional images of the membranes listed in Table. 4-2. 80

Fig. 4-5 VMD performance and LEPw of hybrid nanocomposite membrane (low SiO2 content) 83

Fig. 4-6 Pure water VMD performance and LEPw for hybrid nanocomposite membranes with high SiO_2 content (7%).....86

Fig. 4-7 Salty water VMD performance for hybrid nanocomposite membranes with high SiO_2 content (7%) 87

Fig. 4-8 Possible mechanism of change for membrane pores with introduction of SiO_2 NPs.....88

Fig. 4-9 Effect of SiO_2 NPs addition of the aggregate size distribution of CNTs.....90

List of tables

Table. 3-1 Top-surface characterizations of membranes with different MWCNTs loadings. 43

Table. 3-2 Comparison of roughness parameter of membrane with/without MWCNTs blending 45

Table. 3-3 Some characteristics of membrane with different MWCNTs loadings 47

Table. 3-4 Tensile properties of membranes with different MWCNTs loadings. 50

Table. 3-5 Comparison of different CNTs applications into MD 55

Table. 4-1 Properties of NPs supplied by the manufactures.. 71

Table. 4-2 Top-surface characterizations of membranes.....79

Table. 4-3 Thickness, finger layer ratio and porosity of membranes 78

Table. 4-4 Tensile properties of membranes with different MWCNTs loadings 81

Table. 4-5 Surface roughness parameters of L7 membranes.....86

Table. 4-6 Related studies about hybrid nano-additives on membrane.....91

Nomenclature

A	membrane sample area
B	geometric factor of pore
C_f	conductivity of feed water
C_p	conductivity of permeated water
l	thickness of membrane
P_f	hydraulic pressure at feed side
P_p	hydraulic pressure at permeate side
R	salt rejection
R_a	average roughness
R_{MAX}	maximum roughness
R_q	root mean square roughness
r_{max}	largest pore size of membrane
t	time
$Tmax$	Maximum temperature
w	weight
θ	contact angle
γ_l	surface tension of liquid
ε	porosity of membrane
ρ	density

Abbreviations

AFM	Atomic Force Microscopy
AGMD	Air-gap membrane distillation
BP	Bucky-paper
CNIM	Carbon nanotubes immobilized membrane
CNT	Carbon nanotube
DCMD	Direct contact membrane distillation
DMAC	N, N-dimethylacetamide
GO	Graphene oxide
LEP	Liquid entry pressure
LEPw	Liquid entry pressure of water
MD	Membrane distillation
MWCNT	Multi-walled carbon nanotube
NPs	Nanoparticles
PVDF	Polyvinylidene fluoride
RO	Reverse osmosis
SEM	Scanning electron microscopy
SGMD	Sweep-gas membrane distillation
TEM	Transmission electron microscopy
VMD	Vacuum membrane distillation

1. Introduction

The scarcity of freshwater has emerged as a threat to sustainable development of human society. With increasing world population, expansion of agriculture irrigation, economic growth and change of living styles, demand of freshwater is continuously rising[1-2]. Meeting the increasing demand of freshwater motivates the search for possible technologies to increase the production and improve the utility of freshwater. As a potential method to enhance freshwater supply, desalination technologies, which rely on the huge seawater reserve of oceans, saline rivers and groundwater, have been gradually gaining importance during the last decades. According to the report from International Desalination Association, the global cumulative desalination capacity has reached 92.5 million m^3/day in 2017[3]. Increasing demand of freshwater and decline of desalination cost have contributed to the continuous expansion of desalination market[4].

Typically, desalination technologies can be divided into evaporation desalination process, such as multi-stage flash and multi-effect distillation, and membrane-based process[4-6]. Reverse osmosis (RO), as the dominating membrane desalination process which accounts for more than 60 % of global desalination market, has been thoroughly studied and considerably improved in the past five decades[4-5]. Comparing with conventional thermal desalination processes, RO shows lower energy consumption and higher production efficiency which contribute to its wide applications. However, RO desalination technology also suffers from different challenges and problems: fouling, lower recovery rate and disposal of concentrated brine[2, 4-5]. To overcome these problems and to further decrease the energy consumption, some alternative desalination technologies are being investigated.

Membrane distillation (MD) is one of such technologies, by which increase of production efficiency and decrease of energy cost are aimed at.

In contrast to RO that is pressure driven, MD is a thermally driven membrane-based process. Due to its unique modular and special hydrophobic microporous membrane, fouling control and high salty reduction are possible[4, 7-8]. Moreover, since MD operates at relatively low temperature (i.e., 30-80 ºC), using low grade heat from renewable energy resources and waste heat for MD is possible. MD could also be coupled with other desalination technologies such as RO to improve desalination efficiencies, thus providing growth potential for its further development[7-8]. As one of the most crucial aspects of MD, design of membranes with excellent performance has been pursued for further development of MD.

In order to improve the freshwater production efficiency of MD process, the membrane with low resistance to mass transfer is preferred[4, 8-9]. High liquid entry pressure of water (LEPw), the pressure threshold at which liquid water would penetrate into pores to cause pore wetting of membranes, low thermal conductivity, which would help reduce heat loss by conduction, and mechanical strength which is essential for the robustness of membranes are also required for successful MD membranes[4, 8]. These key factors are closely related to the membrane structure and morphology. Surface properties (e.g. pore size, its distribution surface porosity and surface roughness), cross-sectional properties (e.g. porosity of membrane, thickness and tortuosity) all inherently affect the mass transfer through membrane, LEP and other membrane properties[9-10]. Various approaches have been investigated with certain successes, to optimize the membrane morphology and

performance. Among those, incorporation of nano-additives into the host polymeric membrane has demonstrated positive impacts on the membrane[4, 10-11].

Loading of nano-additives contributes to better MD performance by increasing porosity and pore size of the membrane[12-14]. In particular, hydrophobic additives increase the hydrophobicity of the membrane surface, which is favored by the MD membrane[14-16]. However, the larger pore size and higher membrane porosity lead to lower LEPw and possible compromise of salt rejection[4,11]. The loading of hydrophilic particles lowers hydrophobicity of the surface and leads to the formation of large pores[12]. Moreover, negative impacts of additives aggregation and the relatively low vapor permeability compared with other modification methods are currently hampering the wider application of nano-additives in MD membrane development[10-11].

As a potential additive into MD membrane, carbon nanotubes (CNTs), with extraordinary mechanical properties and intrinsic channel structure, have proven their effectiveness to improve the membrane performance[15, 17-18]. In this work, the attention was focused on the CNT additives and their effects on membrane. To obtain deeper understanding of the effects of CNTs incorporation on the membrane structure and other properties was the main objective of this study. In the chapter 3, MWCNTs would be introduced into membrane and relative characteristics would be tested in order to prove the MWCNTs' effects on membranes. In the latter part of the thesis, different silicon dioxide nano-additives were incorporated together with CNTs and their synergistic effects were investigated. It should be noted that all the membranes fabricated in this work had to satisfy the following requirements:

- High salt rejection (above 99.9%) when a large number of nano-additives are incorporated;
- Sufficiently high vapor permeation rate without significant LEP compromise (Maintained above 20 Psi) at relatively low feed temperature;
- High mechanical strength can be maintained during operation even at high additives loading.

Reference

1. Ercin, A. E.; Hoekstra, A. Y., Water footprint scenarios for 2050: A global analysis. Environment International 2014, 64, 71-82.
2. Mekonnen, M. M.; Hoekstra, A. Y., Four billion people facing severe water scarcity. Science Advances 2016, 2 (2), e1500323.
3. Association, I. D., IDA Desalination Yearbook 2017-2018. 2017.
4. Ghaffour, N.; Missimer, T. M.; Amy, G. L., Technical review and evaluation of the economics of water desalination: current and future challenges for better water supply sustainability. Desalination 2013, 309, 197-207.
5. Drioli, E.; Ali, A.; Macedonio, F., Membrane distillation: Recent developments and perspectives. Desalination 2015, 356, 56-84.
6. Shannon, M. A.; Bohn, P. W.; Elimelech, M.; Georgiadis, J. G.; Mariñas, B. J.; Mayes, A. M., Science and technology for water purification in the coming decades. Nature 2008, 452 (7185), 301.
7. Zarzo, D.; Prats, D., Desalination and energy consumption. What can we expect in the near future? Desalination 2018, 427, 1-9.

8. Burn, S.; Hoang, M.; Zarzo, D.; Olewniak, F.; Campos, E.; Bolto, B.; Barron, O., Desalination techniques—a review of the opportunities for desalination in agriculture. Desalination 2015, 364, 2-16.
9. Amy, G.; Ghaffour, N.; Li, Z.; Francis, L.; Linares, R. V.; Missimer, T.; Lattemann, S., Membrane-based seawater desalination: Present and future prospects. Desalination 2017, 401, 16-21.
10. González, D.; Amigo, J.; Suárez, F., Membrane distillation: Perspectives for sustainable and improved desalination. Renewable and Sustainable Energy Reviews 2017, 80, 238-259.
11. Khayet, M., Membranes and theoretical modeling of membrane distillation: A review. Advances in Colloid and Interface Science 2011, 164 (1-2), 56-88.
12. Eykens, L.; De Sitter, K.; Dotremont, C.; Pinoy, L.; Van der Bruggen, B., Membrane synthesis for membrane distillation: A review. Separation and Purification Technology 2017, 182, 36-51.
13. Baghbanzadeh, M.; Rana, D.; Lan, C. Q.; Matsuura, T., Effects of inorganic nano-additives on properties and performance of polymeric membranes in water treatment. Separation & Purification Reviews 2016, 45 (2), 141-167.
14. Baghbanzadeh, M.; Rana, D.; Lan, C. Q.; Matsuura, T., Effects of hydrophilic silica nanoparticles and backing material in improving the structure and performance of VMD PVDF membranes. Separation and Purification Technology 2016, 157, 60-71.
15. Hou, D.; Dai, G.; Fan, H.; Wang, J.; Zhao, C.; Huang, H., Effects of calcium carbonate nano-particles on the properties of PVDF/nonwoven fabric flat-sheet composite membranes for direct contact membrane distillation. Desalination 2014, 347, 25-33.

16. Efome, J. E.; Baghbanzadeh, M.; Rana, D.; Matsuura, T.; Lan, C. Q., Effects of superhydrophobic SiO_2 nanoparticles on the performance of PVDF flat sheet membranes for vacuum membrane distillation. Desalination 2015, 373, 47-57.
17. Tijing, L. D.; Woo, Y. C.; Shim, W.-G.; He, T.; Choi, J.-S.; Kim, S.-H.; Shon, H. K., Superhydrophobic nanofiber membrane containing carbon nanotubes for high-performance direct contact membrane distillation. Journal of Membrane Science 2016, 502, 158-170.
18. Razmjou, A.; Arifin, E.; Dong, G.; Mansouri, J.; Chen, V., Superhydrophobic modification of TiO_2 nanocomposite PVDF membranes for applications in membrane distillation. Journal of Membrane Science 2012, 415, 850-863.
19. Silva, T. L.; Morales-Torres, S.; Figueiredo, J. L.; Silva, A. M., Multi-walled carbon nanotube/PVDF blended membranes with sponge-and finger-like pores for direct contact membrane distillation. Desalination 2015, 357, 233-245.
20. Gethard, K.; Sae-Khow, O.; Mitra, S., Water desalination using carbon-nanotube-enhanced membrane distillation. ACS Applied Materials & Interfaces 2010, 3 (2), 110-114.

2. Literature review

Freshwater, as a critical resource on earth, is suffering from severe scarcity because of the rapid growth of global population and expansion of economy. According to the related research, there are four billion people experiencing different levels of water scarcity[1]. With restricted direct access to freshwater resources and limited renewable ability of freshwater, an impending requirement to find alternative approaches to supply more freshwater has emerged. As one of such approaches, desalination technology has attracted much attention from society as the most promising method. The seawater in oceans, which accounts for more than 97 % of the global water reserves[2-3], in addition to the broadly distributed brackish waters, provides a promising solution to the worldwide freshwater scarcity and hopeful future for extensive application of different desalination technologies.

Among different existing desalination processes, the membrane-based desalination process dominates the commercial market, accounting for more than 60 % of the global capacity[4-5]. Reverse osmosis (RO), as currently the most prevalent desalination technology, however, meets several challenges which impede the further development of this technology. Relatively high energy consumption, low recovery for sea water desalination, and severe membrane fouling negatively influence the application of RO process[6]. To address these limitations, membrane distillation (MD) has been investigated as a stand-alone process or in a hybrid system with RO. Compared with RO which is pressure driven, MD is a thermally driven process involving vapor-liquid phase equilibrium. By employing porous hydrophobic membrane in MD, only water vapor can pass through the membrane due to vapor pressure difference between two sides of the membrane while non-volatile components are retained at the feed side. Hence, MD process could

achieve 100 % theoretical salt rejection[7-8]. As well, comparing with traditional distillation desalination technologies, MD could operate at relatively low temperature[9].

Even though MD was introduced as a novel separation technology in the 1960s, it has not yet been widely accepted by the commercial market of desalination[10]. One major factor hindering the commercialization of MD is the unfavorable energy consumption compared with the mature RO technology[8, 10-11]. The other factor is the unsatisfactory membrane durability which does not allow to sustain excellent performance for long-term operation[10, 12]. For improving the energy efficiency of the MD process, coupling of MD with renewable energies has been studied to prove its effectiveness[8, 11, 13]. As well, different membrane improvement methods, including different MD configurations, fouling reduction, and numerical simulations in module and system design have been investigated to improve the efficiency of MD for its further application[7, 9-10, 14]. This thesis is focused on the membrane improvement by way of the incorporation of integrated nano-additives into the polymeric membrane, attempting to gain deep understanding of the effects of membrane structure on MD performance.

2.1. Membrane distillation (MD)

2.1.1. Membrane distillation configurations

As a thermally driven process, MD can separate non-volatile solutes, such as salt, from aqueous solution. Vapor transfers through the membrane whereas liquid water and dissolved components are retained on the feed side. The Fig. 2-1 schematically illustrates the principle of the MD process. Hydrophobic membrane, as a barrier, plays the crucial role to separate the salt from feed saline

water. According to the vapor collection methods on the permeate side, MD is classified into four basic configurations[8, 10]: Direct contact MD (DCMD), air-gap MD (AGMD), vacuum MD (VMD), and sweep-gas MD (SGMD). Among these configurations, DCMD is the most popular due to its simplest construction[10]. There are also some modified MD configurations aiming to increase energy efficiency and production of unsalted vapor, such as vacuum-enhanced DCMD , vacuum-multi-effect MD, and so on. Fig. 2-2 is the schematic representation of four basic MD configurations.

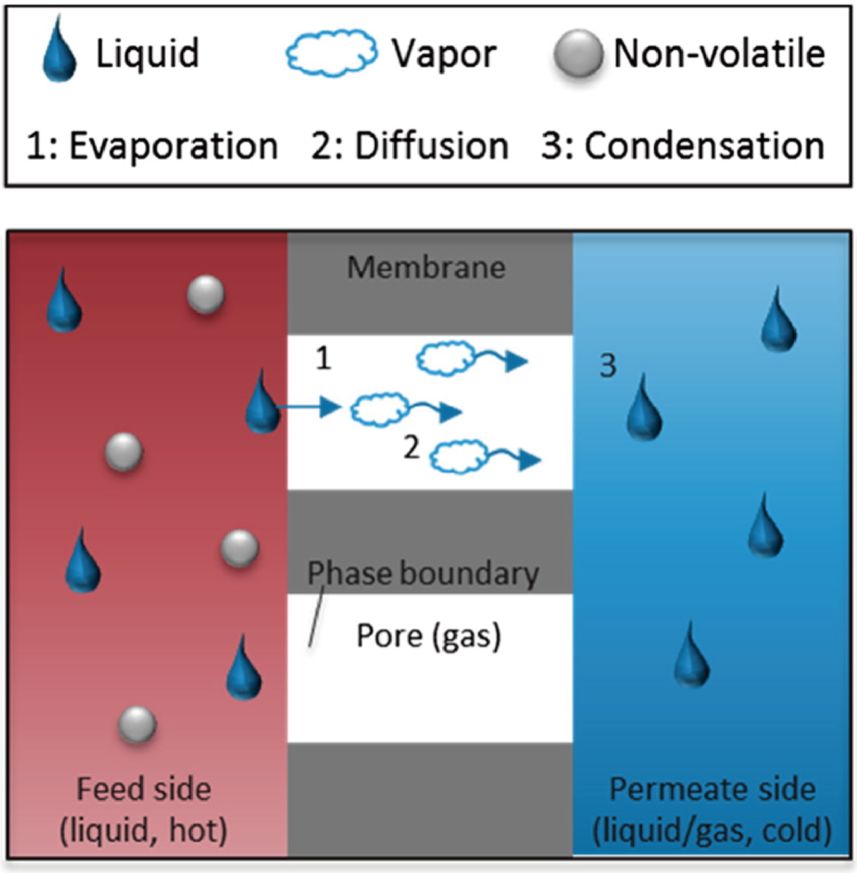

Fig. 2-1 Schematic principles of vapor transport in MD process[15].

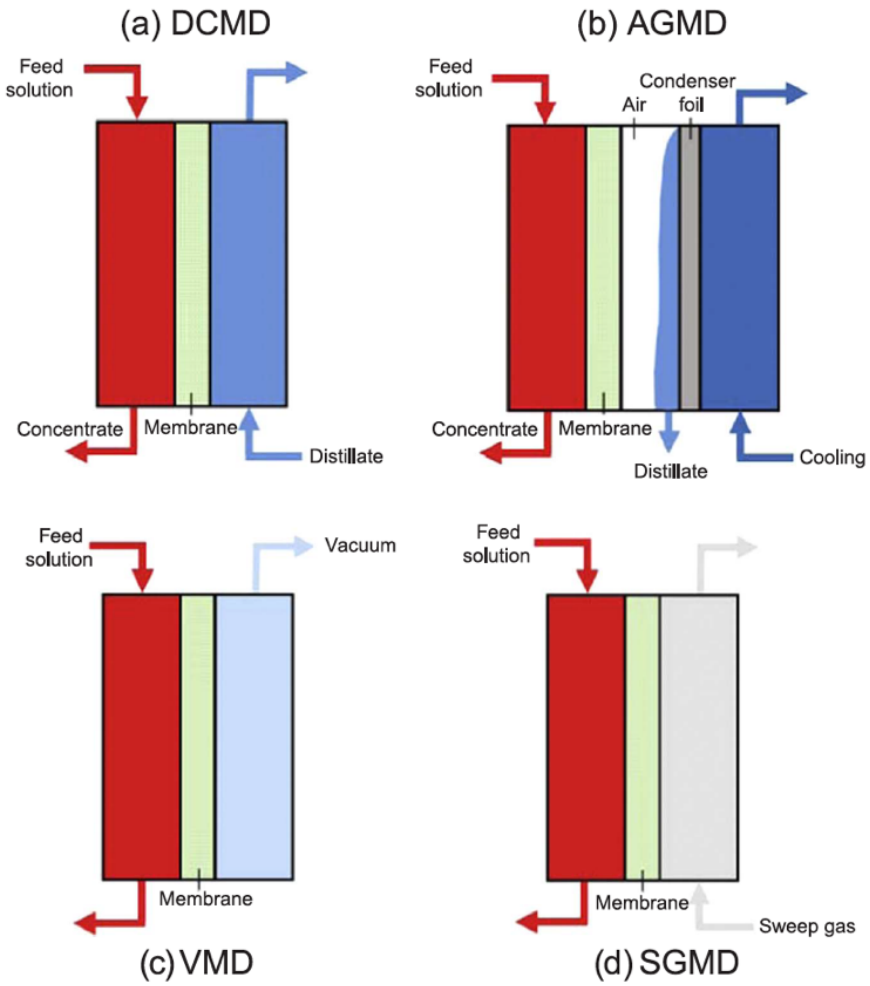

Fig. 2-2 Schematic diagram of four basic MD configuration[8].

DCMD, the simplest construction, has been widely investigated in laboratory-scale studies. The warm feed solution is in direct contact with hydrophobic surface of the membrane and the cold water contacts the other side of membrane to condense the permeating vapor. Despite its simple configuration, DCMD has a drawback of conductive heat loss through the thin membrane[8, 10]. DCMD has been widely used to desalinate different salty water supplies[16-20]. DCMD has also been applied to separate aqueous solutions other than saline water, such as production of apple juice with high concentration[21], treatment of olive wastewater[22], treating effluent solution

containing dye[23], and so on. But, with low energy efficiency, the application potential for DCMD was not high in the commercial market[10].

As shown in Fig. 2-2, an air gap is interposed between the membrane and cold condensation surface in AGMD configuration. Unlike DCMD, the vapor, evaporated at the feed side, passes through the membrane and air gap, and condenses at the cold surface rather than directly entering the cold liquid. The presence of air gap between the membrane and the condensation surface reduces the conductive heat loss, which, however, becomes the cause of lower transmembrane flux than DCMD[8, 10]. As an energy-efficient MD process, AGMD configuration is preferred in the commercial desalination market[24-26]. Apart from desalination purpose, AGMD is also suitable to separate some organic substances, such as alcohol, which will be the cause of wetting problems in DCMD configuration[25, 27].

In VMD configuration, a vacuum or reduced pressure condition is created at permeate side using vacuum pump. Due to reduced vapor pressure at permeate side, VMD configuration exhibits less mass transfer resistance than other MD configurations[10]. However, not only a vacuum pump, but also an external condenser is required in VMD configuration[10]. And also, comparing with other MD configurations, VMD has higher probability of pore wetting and fouling[7]. As for the application of VMD, like AGMD, it is also suitable to separate organic compounds from aqueous system apart from desalination purpose[28-31].

As for SGMD, a cold inert gas is introduced as vapor carrier at permeate side. The vapor, after passing through membrane is taken away from the membrane module and condensed in an external cold trap. Due to sweep inert gas, the vapor pressure at the permeate side is reduced contributing

to a greater driving force for vapor transport[10]. However, the requirement of external condenser and sweep gas causes extra investment and energy consumption like VMD configuration. Although least employed for MD, SGMD is widely investigated for different separation purposes[32-35].

Among these four configurations, DCMD, due to its simplest structure, undoubtedly, is the most popular MD setup in laboratory-scale researches. However, compared with other configurations, high energy loss retards the development of DCMD. In this work, VMD configuration is chosen. External vacuum pump and liquid nitrogen are employed to generate the require vacuum condition on the permeate side and to condense the produced vapor.

2.1.2. Configurations of MD modules

There are three common configurations of MD modules: plate and frame module, tubular module for hollow fiber membrane, and spiral wound module as shown in Fig. 2-3.

The plate and frame module, which is used for all the four basic MD configurations, is readily constructed and widely employed in the laboratory investigation[10]. This module is appropriate for flat sheet membrane, which can be easily fabricated. But, compared with tubular module, plate and frame module has relative smaller effective area[10]. In this work, a frame module was used with fabricated flat sheet membranes.

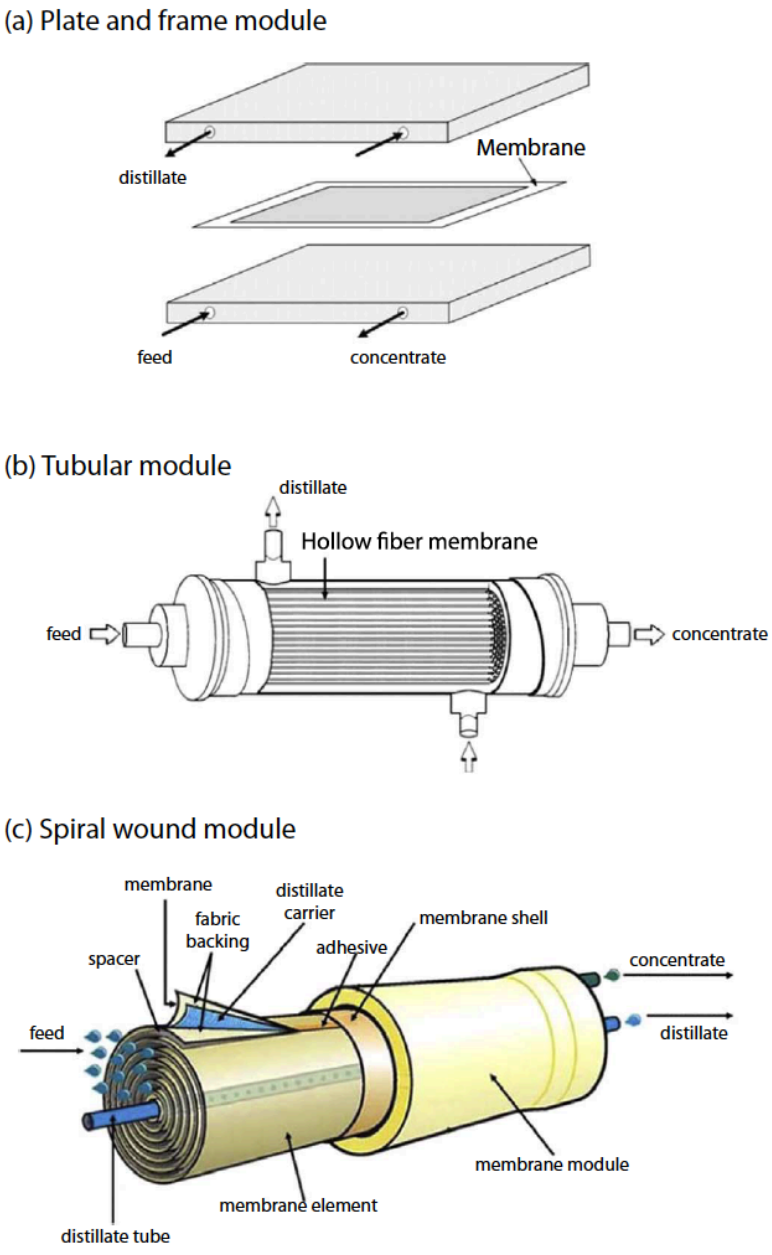

Fig. 2-3 Schematic of three typical MD modules[8].

With the larger surface area, hollow fiber installed tubular module offers a promising potential for commercial application for desalination[36]. This module is suitable for DCMD, VMD and SGMD[10]. In spiral wound modules, numerous membranes are enveloped and rolled around a central collective pipe as exhibited in Fig. 2-3[8, 36]. This module also has a large surface area which is

favored by separation process. However, unlike wide applications of hollow fiber based tubular module, this module is mainly employed for AGMD[10].

2.1.3. Membranes for MD

As mentioned above, porous membranes employed in the MD process retains salt and other non-volatile solutes in the feed stream. Driven by vapor pressure difference between feed and permeate side, vapor is transferred through the porous membrane which not only serves as a physical barrier, but also plays an important role in heat transfer. As one of the crucial factors in MD process, structures and properties of membrane directly affect the performance of the process. MD membranes should have good thermal stability and strong chemical resistance to feed solution[7]. The properties required for MD membranes are listed below[7, 10, 37-38]:

- Appropriate membrane thickness as a compromise between thermal resistance and vapor permeability. As membrane becoming thicker, the mass transfer through the membrane decreases whereas thermal resistance will increase contributing to less energy loss.
- Reasonably large pore size and narrow pore size distribution, which can permit the vapor passing but forbid the penetration of liquid water into the pore. Also, high liquid entry pressure (LEP) is required for MD membrane. LEP is defined as the minimum hydraulic pressure on the feed side which allows the liquid penetration through the membrane. The equation below is often used to evaluate the LEP:

$$LEP = P_f - P_p = \frac{-2\ B\ \gamma_l\ cos\theta}{r_{max}} \quad (1)$$

  Where P_f and P_p are the hydraulic pressure at the feed and permeate side respectively. B is a geometric factor of pore which equals to 1 for cylindrical pores. γ_l indicates the surface tension

of liquid. θ represents the contact angle between liquid and membrane surface. r_{max} is the largest pore size of membrane top surface.

LEP is a crucial characteristic to evaluate the pore wetting resistance. Membrane with high LEP has a great potential for long-term operation. High LEP could be achieved by high hydrophobicity and small maximum pore size at the membrane surface. However, small maximum pore size on surface is often accompanied by small mean pore size, which is not favored by MD. Hence, in order to satisfy both small maximum pore size and large mean pore size, a narrow pore size distribution is required.

- High porosity (void volume fraction of membrane) and small tortuosity (which reflects the deviation of the pore structure from straight cylindrical pores). Vapor flux through membrane directly relates to pore size, porosity and tortuosity. Large pore size, high porosity and small tortuosity will contribute to high vapor flux. And also, high porosity leads to increased thermal resistance, contributing to higher energy efficiency. However, in some cases, weakening of mechanical properties is attributed to high porosity of membrane. Therefore, reasonably high porosity of membrane is favored in MD.
- Low thermal conductivity and fouling tendency. High thermal conductivity will decrease temperature difference between two sides of membrane contributing to low vapor flux. Small transmembrane pressure of MD membrane diminishes the possibility of membrane fouling. But, in industrial applications of MD, the suspended particles and bacteria in feed may still cause severe fouling problems at the feed side of the membrane, which negatively affect the long-time stability of MD.
- High chemical and thermal stability. These two key factors are directly related to long-term stability of membrane in practical application of MD.

Typically, polymeric membranes, including polytetrafluoroethylene (PTFE) membrane, polypropylene (PP) membrane, polyvinylidene fluoride (PVDF) membrane are most commonly used in MD. Sometimes, ceramic membranes are also used for MD. But limited by high cost, ceramic membrane does not attract as strong attention as polymeric membrane[15]. In order to fabricate porous hydrophobic polymeric membrane, different membrane fabrication methods are employed. Common fabricating methods include phase inversion method, stretching method, sintering method and electrospinning method.

Among these methods, sintering and stretching methods are suitable to produce PTFE membrane since it does not require solvent[10]. In the sintering process, polymer powder is pressed into film or plate at temperature below melting point. By contrast, polymer powder in stretching method is heated above melting point and extruded into desired films[10]. Compared with these two methods, in the phase inversion and electrospinning method, solvent is necessary to dissolve polymer. Phase inversion method, based on a transition between two phases, is induced by polymer solubility difference. Among different phase inversion methods, nonsolvent induced phase inversion is the most popular, in which polymer solidification is induced by the solvent/nonsolvent exchange in the coagulation bath. Electrospinning is a promising membrane fabrication method which can produce unique nanomaterials called nanofibers[39]. As polymer solution, or polymer melt, is ejected from the syringe, nanofibers are formed under the effect of the high electric field. Compared with sintering, stretching and phase inversion method, electrospinning, as a novel fabrication method, has high pore interconnectivity and relatively uniform pore size distribution, which provides more choices for membrane fabrication[39].

As mentioned above, material and structure of membrane govern the MD performance. Besides the exploration of novel membrane fabrication method, some feasible membrane modification methods have been investigated, such as the application of some additives, plasma or chemical modification on membrane surface and so on[7, 15]. Incorporation of additives into the membrane is the most readily available approach to modify membranes when they are fabricated by phase inversion or electrospinning. Common additives blended into casting or spinning solutions include water[40], lithium chloride[38, 41], some inorganic particles, like silicon dioxide (SiO_2)[42-43], copper oxide (CuO)[44], and carbon nanotubes (CNTs)[45-46]. These additives can change the membrane structure and morphology, leading to enhancement of membrane performances.

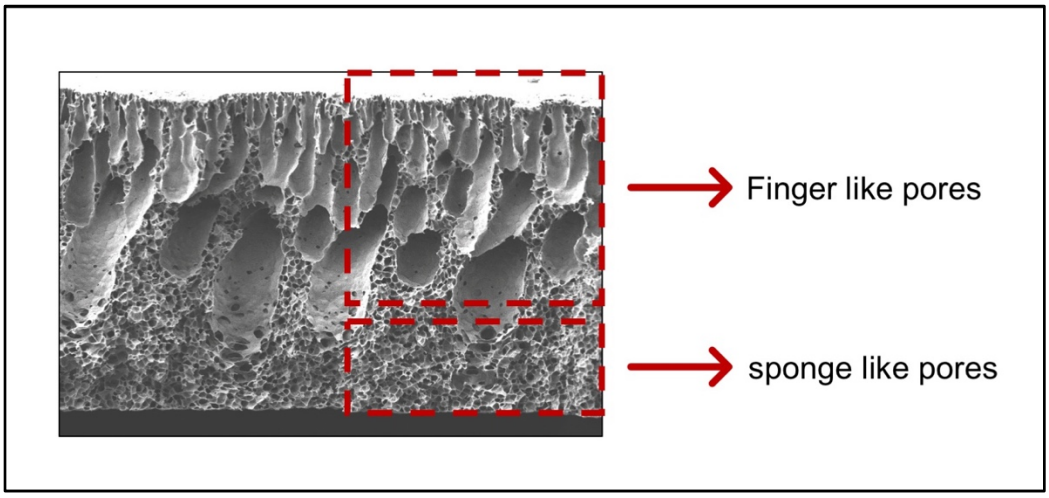

Fig. 2-4 Typical cross-sectional SEM pictures of membrane

In the phase inversion process, the rate of solvent/nonsolvent exchange (or the rate of phase inversion) determines the pore structure of the membrane[47-50]. Usually, membranes fabricated by the phase inversion method have an asymmetric structure with a top skin layer supported by porous sublayer as shown in in the Fig. 2-4[44]. Fast phase exchange contributes to the formation of finger-like pores and also to the increase in membrane porosity. On the other hand, low phase inversion

rate will promote the sponge-like pores formation with decrease in membrane porosity. The primary role of the additives is to adjust the phase inversion rate[47, 49] and change surface roughness and hydrophobicity aiming at the improvement of membrane performance[40, 51]. Many different additives have been tested on their effectiveness, expecting their favorable impacts on membrane's structure and performance. Among them, carbon nanotubes (CNTs) are an attractive option as additives due to its unique structure[52-53].

2.2. Carbon nanotubes and their application into MD.

2.2.1. Characteristics of Carbon nanotubes

Carbon nanotubes, as a novel carbon material, has been thoroughly studied since it was discovered in 1991[54]. Carbon nanotubes can be classified into single-walled carbon nanotubes (SWCNTs) and multi-walled carbon nanotubes (MWCNTs). Both of them were proven to have remarkable electronic and mechanical properties and high thermal conductivity by many researches[55-57]. Excellent properties of CNTs, undoubtedly, provide a promising future for further application of these novel materials. Besides, in the field of water treatment, the intrinsic hollow structures of CNTs, which enable fast water transport, have attracted growing attention[52-53].

It was found both by experiment and computer simulation that the hydrophobic channels of uncapped CNTs allow the fast transportation of water through their channels[58-62]. The inner diameters of CNTs are usually less than 10 nm and the velocity of water permeation through the channels is independent of the length of CNTs channels[59]. Furthermore, with the small channel diameter CNTs can impede the permeation of some ions, thus enabling salt rejection[63-68].

CNTs or functionalized CNTs/polymer composites also exhibit improved mechanical properties[55, 69]. As well, addition of CNTs into polymeric membrane improved greatly membrane's mechanical properties[70-73].

2.2.2. CNTs application on MD

There are three typical approaches of CNTs utilized to improve the membrane performance in MD. The most attractive way is called CNTs self-supporting bucky-paper membrane (BP membrane). There are a series of researches focusing on this approach[74-76]. CNTs BP membrane, as one of inorganic membranes, does not require any polymer participation. Van der Waals force between CNTs align them together to make the membrane self-supporting. Compared with conventional polymeric membranes for MD, CNTs BP membrane has smaller pore sizes of just about 25 nm and larger porosity. Narrow pore size distribution is also a characteristic of BP membrane. However, relatively low salt rejection and weak mechanical stability of BP membrane have impeded its further application for long-term MD process. Even though modification of CNTs and combination with other polymeric membranes have been attempted to make the lifecycle of BP membrane longer, vapor flux of BP membrane was inadequately low.

Directly immobilizing CNTs on membrane pores is another attracting method to use CNTs in membrane fabrication[77-79]. The membrane is called CNTs immobilized membrane (CNIM). Immobilized CNTs enhance the vapor transfer through membrane and also contribute to higher salt rejection. Salt adsorption capability and hydrophobic surface of CNTs provide fast transport pathway for water vapor, thus facilitating the water vapor permeation through membrane. As well,

functionalization of CNTs was found to magnify the improvement of membrane perormance[78]. However, low salt reduction compared with other MD membranes and possible CNTs leakage due to weak interaction between CNTs and polymer are the main problems of CNIM[80].

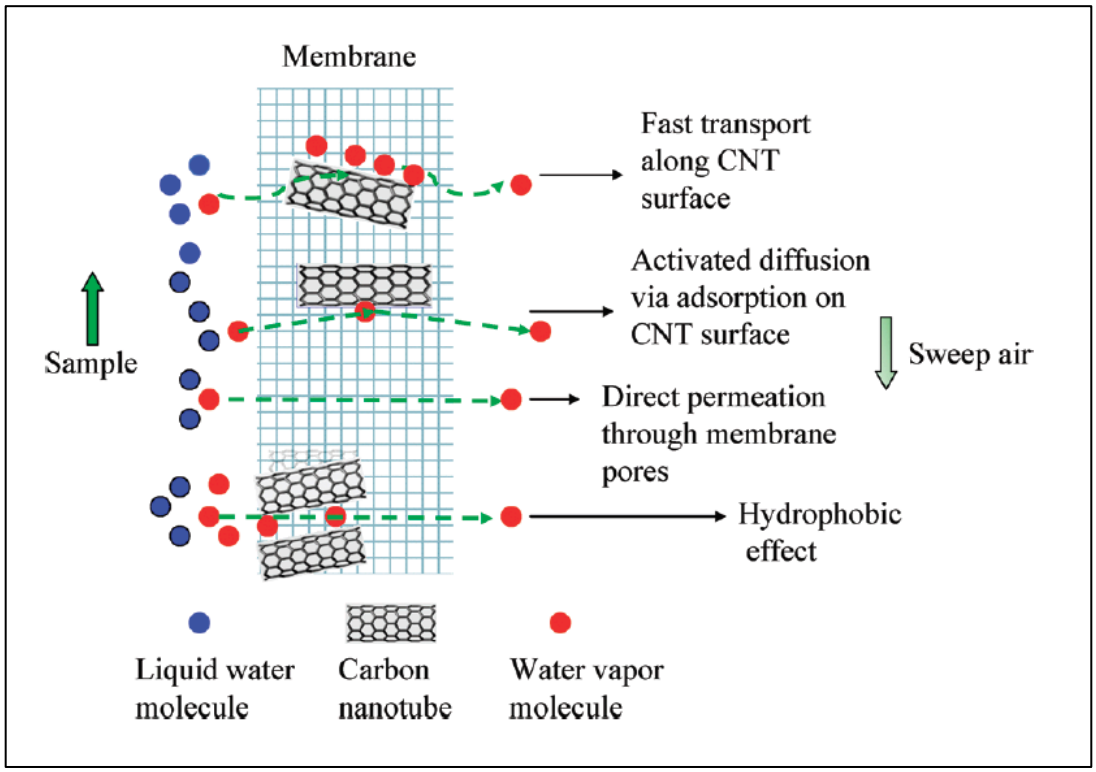

Fig. 2-5 Mechanisms of MD in the presence of CNTs[77].

BP membrane and CNIM exhibit not only poor MD performance but also their fabrication procedure is complicated. Directly introducing CNTs into membrane casting solution appears to be a promising approach to apply CNTs for membrane fabrication. When membrane is fabricated by the phase inversion technique, CNTs blended in the casting dope mainly changes the porous structures of the membrane resulting in better MD performance[45]. When electro-spun, CNTs incorporation leads to higher hydrophobicity and better mechanical properties[46, 80]. Indeed, the

vapor transport through membrane has been facilitated due to the presence of CNTs and their aggregates[46].

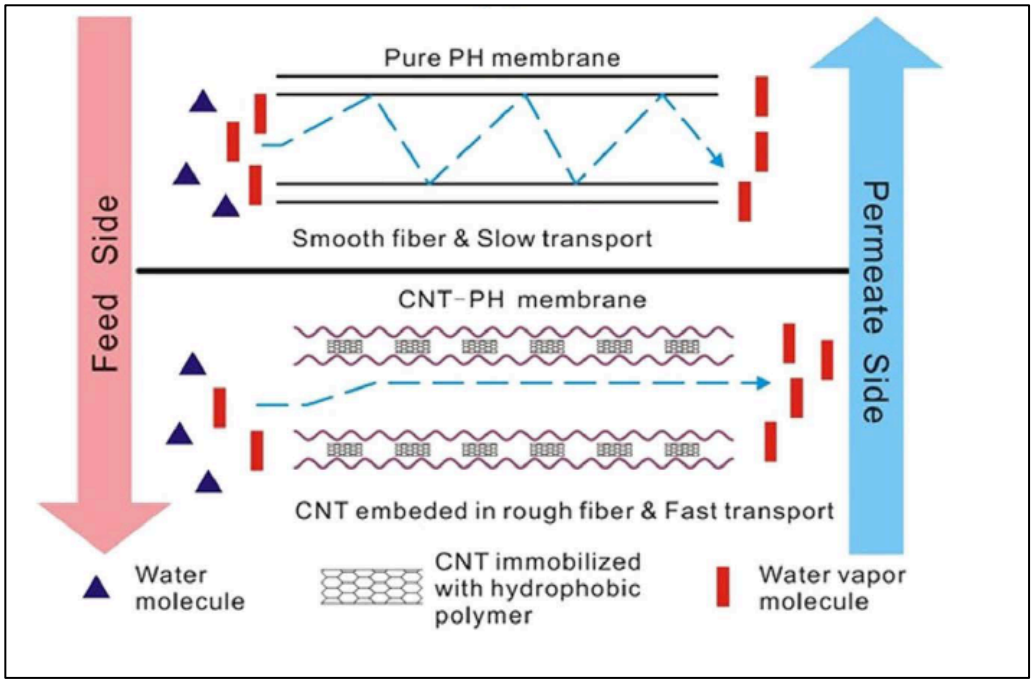

Fig. 2-6 Effect of increased roughness on vapor transport in the CNTs membranes[46].

2.2.3. Comparison of CNTs with other inorganic additives.

Even though CNTs have many excellent features, their use in membrane fabrication is rather limited because of their high cost. Water is another common additive to the casting dope of the phase inversion method[40, 81]. With the added water, pores size and porosity are both enhanced. Lithium chloride (LiCl) is another additive into the casting solution, which can increase the phase inversion rate contributing to higher porosity[41, 82]. Inorganic particles, such as SiO_2[41-42] and TiO_2[82], are attracting more attention than water and lithium chloride.

Loading ratio, particle diameter, and particle hydrophobicity all affect the membrane structure but their effects reported in the literature seem sometimes contradictory[51]. According to our earlier works, addition of hydrophilic particles will result in longer finger like pores and higher porosity[43-44]. Hydrophobic particles increase the pore size and the contact angle[42]. Integration of particles with different hydrophobicity has synergic effects on membrane performance[83]. Other effects of additives are; 1) The particles could serve as extra nucleation agent which could elevate the polymer crystallization rate. 2) Disrupting compatibility between solvent and polymer, phase inversion is facilitated by the additives. 3) By increasing viscosity, phase inversion process is delayed. Therefore, the choice of additives and their amount should be based on the compromise of these factors. Deeper understanding of different effects of the additives on membrane structure, properties and performance is indispensable for MD membranes to be fully accepted in the desalination market.

Compared with other nano-particles, CNTs are unique with their length reaching more than 1 μm. Also, their unique hydrophobic channels can permit fast water transport which is fundamentally important for them to be used in water treatment process. With many desired properties, CNTs are expected to exhibit remarkable improvement of membrane, even though severe aggregation of CNTs and relatively high cost of its manufacture and functionalization may impede their further utilization as additives in the membrane[52-53]. Existing studies about CNTs application on MD are limited as mentioned above. Also, the potential of CNTs integrated with other additives as hybrid fillers introduced into membrane has not been thoroughly explored[83]. CNTs, as an attractive additive for membrane in MD, require further and deeper studies for their better utilization.

Reference

1. Mekonnen, M. M.; Hoekstra, A. Y., Four billion people facing severe water scarcity. Science Advances 2016, 2 (2), e1500323.
2. Burn, S.; Hoang, M.; Zarzo, D.; Olewniak, F.; Campos, E.; Bolto, B.; Barron, O., Desalination techniques—a review of the opportunities for desalination in agriculture. Desalination 2015, 364, 2-16.
3. Elimelech, M.; Phillip, W. A., The future of seawater desalination: energy, technology, and the environment. Science 2011, 333 (6043), 712-717.
4. Ghaffour, N.; Missimer, T. M.; Amy, G. L., Technical review and evaluation of the economics of water desalination: current and future challenges for better water supply sustainability. Desalination 2013, 309, 197-207.
5. Shannon, M. A.; Bohn, P. W.; Elimelech, M.; Georgiadis, J. G.; Mariñas, B. J.; Mayes, A. M., Science and technology for water purification in the coming decades. Nature 2008, 452 (7185), 301.
6. Drioli, E.; Ali, A.; Macedonio, F., Membrane distillation: Recent developments and perspectives. Desalination 2015, 356, 56-84.
7. González, D.; Amigo, J.; Suárez, F., Membrane distillation: Perspectives for sustainable and improved desalination. Renewable and Sustainable Energy Reviews 2017, 80, 238-259.
8. Tijing, L. D.; Woo, Y. C.; Choi, J.-S.; Lee, S.; Kim, S.-H.; Shon, H. K., Fouling and its control in membrane distillation—a review. Journal of Membrane Science 2015, 475, 215-244.
9. Camacho, L. M.; Dumée, L.; Zhang, J.; Li, J.-d.; Duke, M.; Gomez, J.; Gray, S., Advances in membrane distillation for water desalination and purification applications. Water 2013, 5 (1), 94-196.

10. Al-Karaghouli, A.; Kazmerski, L. L., Energy consumption and water production cost of conventional and renewable-energy-powered desalination processes. Renewable and Sustainable Energy Reviews 2013, 24, 343-356.
11. Alklaibi, A. M.; Lior, N., Membrane-distillation desalination: Status and potential. Desalination 2005, 171 (2), 111-131.
12. Qtaishat, M. R.; Banat, F., Desalination by solar powered membrane distillation systems. Desalination 2013, 308, 186-197.
13. Hitsov, I.; Maere, T.; De Sitter, K.; Dotremont, C.; Nopens, I., Modelling approaches in membrane distillation: a critical review. Separation and Purification Technology 2015, 142, 48-64.
14. Eykens, L.; De Sitter, K.; Dotremont, C.; Pinoy, L.; Van der Bruggen, B., Membrane synthesis for membrane distillation: A review. Separation and Purification Technology 2017, 182, 36-51.
15. Singh, D.; Sirkar, K. K., Desalination of brine and produced water by direct contact membrane distillation at high temperatures and pressures. Journal of Membrane Science 2012, 389, 380-388.
16. Lin, S.; Yip, N. Y.; Elimelech, M., Direct contact membrane distillation with heat recovery: Thermodynamic insights from module scale modeling. Journal of Membrane Science 2014, 453, 498-515.
17. Boubakri, A.; Hafiane, A.; Bouguecha, S. A. T., Direct contact membrane distillation: capability to desalt raw water. Arabian Journal of Chemistry 2017, 10, S3475-S3481.
18. Fard, A. K.; Rhadfi, T.; Khraisheh, M.; Atieh, M. A.; Khraisheh, M.; Hilal, N., Reducing flux decline and fouling of direct contact membrane distillation by utilizing thermal brine from MSF desalination plant. Desalination 2016, 379, 172-181.

19. Li, J.; Guan, Y.; Cheng, F.; Liu, Y., Treatment of high salinity brines by direct contact membrane distillation: Effect of membrane characteristics and salinity. Chemosphere 2015, 140, 143-149.
20. Laganà, F.; Barbieri, G.; Drioli, E., Direct contact membrane distillation: modelling and concentration experiments. Journal of Membrane Science 2000, 166 (1), 1-11.
21. Kiai, H.; García-Payo, M.; Hafidi, A.; Khayet, M., Application of membrane distillation technology in the treatment of table olive wastewaters for phenolic compounds concentration and high quality water production. Chemical Engineering and Processing: Process Intensification 2014, 86, 153-161.
22. Mokhtar, N.; Lau, W.; Ismail, A.; Youravong, W.; Khongnakorn, W.; Lertwittayanon, K., Performance evaluation of novel PVDF–Cloisite 15A hollow fiber composite membranes for treatment of effluents containing dyes and salts using membrane distillation. RSC Advances 2015, 5 (48), 38011-38020.
23. Hanemaaijer, J. H.; van Medevoort, J.; Jansen, A. E.; Dotremont, C.; van Sonsbeek, E.; Yuan, T.; De Ryck, L., Memstill membrane distillation–a future desalination technology. Desalination 2006, 199 (1-3), 175-176.
24. Meindersma, G.; Guijt, C.; De Haan, A., Desalination and water recycling by air gap membrane distillation. Desalination 2006, 187 (1-3), 291-301.
25. Guillén-Burrieza, E.; Blanco, J.; Zaragoza, G.; Alarcón, D.-C.; Palenzuela, P.; Ibarra, M.; Gernjak, W., Experimental analysis of an air gap membrane distillation solar desalination pilot system. Journal of Membrane Science 2011, 379 (1-2), 386-396.
26. Kujawska, A.; Kujawski, J. K.; Bryjak, M.; Cichosz, M.; Kujawski, W., Removal of volatile organic compounds from aqueous solutions applying thermally driven membrane processes. 2. Air gap membrane distillation. Journal of Membrane Science 2016, 499, 245-256.

27. Izquierdo-Gil, M.; Jonsson, G., Factors affecting flux and ethanol separation performance in vacuum membrane distillation (VMD). Journal of Membrane Science 2003, 214 (1), 113-130.
28. Banat, F.; Al-Asheh, S.; Qtaishat, M., Treatment of waters colored with methylene blue dye by vacuum membrane distillation. Desalination 2005, 174 (1), 87-96.
29. Criscuoli, A.; Zhong, J.; Figoli, A.; Carnevale, M.; Huang, R.; Drioli, E., Treatment of dye solutions by vacuum membrane distillation. Water Research 2008, 42 (20), 5031-5037.
30. Zhang, Y.; Li, M.; Wang, Y.; Ji, X.; Zhang, L.; Hou, L., Simultaneous concentration and detoxification of lignocellulosic hydrolyzates by vacuum membrane distillation coupled with adsorption. Bioresource Technology 2015, 197, 276-283.
31. García-Payo, M.; Rivier, C.; Marison, I.; Von Stockar, U., Separation of binary mixtures by thermostatic sweeping gas membrane distillation: II. Experimental results with aqueous formic acid solutions. Journal of Membrane Science 2002, 198 (2), 197-210.
32. Xie, Z.; Duong, T.; Hoang, M.; Nguyen, C.; Bolto, B., Ammonia removal by sweep gas membrane distillation. Water Research 2009, 43 (6), 1693-1699.
33. Khayet, M.; Cojocaru, C., Artificial neural network model for desalination by sweeping gas membrane distillation. Desalination 2013, 308, 102-110.
34. Shirazi, M. M. A.; Kargari, A.; Tabatabaei, M.; Ismail, A. F.; Matsuura, T., Concentration of glycerol from dilute glycerol wastewater using sweeping gas membrane distillation. Chemical Engineering and Processing: Process Intensification 2014, 78, 58-66.
35. Curcio, E.; Drioli, E., Membrane distillation and related operations—a review. Separation and Purification Reviews 2005, 34 (1), 35-86.
36. Khayet, M.; Matsuura, T.; Mengual, J.; Qtaishat, M., Design of novel direct contact membrane distillation membranes. Desalination 2006, 192 (1-3), 105-111.

37. Khayet, M., Membranes and theoretical modeling of membrane distillation: A review. Advances in Colloid and Interface Science 2011, 164 (1-2), 56-88.
38. Ahmed, F. E.; Lalia, B. S.; Hashaikeh, R., A review on electrospinning for membrane fabrication: challenges and applications. Desalination 2015, 356, 15-30.
39. Khayet, M.; Khulbe, K.; Matsuura, T., Characterization of membranes for membrane distillation by atomic force microscopy and estimation of their water vapor transfer coefficients in vacuum membrane distillation process. Journal of Membrane Science 2004, 238 (1-2), 199-211.
40. Wu, B.; Li, K.; Teo, W., Preparation and characterization of poly (vinylidene fluoride) hollow fiber membranes for vacuum membrane distillation. Journal of Applied Polymer Science 2007, 106 (3), 1482-1495.
41. Efome, J. E.; Baghbanzadeh, M.; Rana, D.; Matsuura, T.; Lan, C. Q., Effects of superhydrophobic SiO_2 nanoparticles on the performance of PVDF flat sheet membranes for vacuum membrane distillation. Desalination 2015, 373, 47-57.
42. Baghbanzadeh, M.; Rana, D.; Lan, C. Q.; Matsuura, T., Effects of hydrophilic silica nanoparticles and backing material in improving the structure and performance of VMD PVDF membranes. Separation and Purification Technology 2016, 157, 60-71.
43. Baghbanzadeh, M.; Rana, D.; Matsuura, T.; Lan, C. Q., Effects of hydrophilic CuO nanoparticles on properties and performance of PVDF VMD membranes. Desalination 2015, 369, 75-84.
44. Silva, T. L.; Morales-Torres, S.; Figueiredo, J. L.; Silva, A. M., Multi-walled carbon nanotube/PVDF blended membranes with sponge-and finger-like pores for direct contact membrane distillation. Desalination 2015, 357, 233-245.

45. An, A. K.; Lee, E.-J.; Guo, J.; Jeong, S.; Lee, J.-G.; Ghaffour, N., Enhanced vapor transport in membrane distillation via functionalized carbon nanotubes anchored into electrospun nanofibres. Scientific reports 2017, 7, 41562.
46. Hou, D.; Dai, G.; Fan, H.; Wang, J.; Zhao, C.; Huang, H., Effects of calcium carbonate nano-particles on the properties of PVDF/nonwoven fabric flat-sheet composite membranes for direct contact membrane distillation. Desalination 2014, 347, 25-33.
47. Van de Witte, P.; Dijkstra, P. J.; Van den Berg, J.; Feijen, J., Phase separation processes in polymer solutions in relation to membrane formation. Journal of Membrane Science 1996, 117 (1-2), 1-31.
48. Fontananova, E.; Jansen, J. C.; Cristiano, A.; Curcio, E.; Drioli, E., Effect of additives in the casting solution on the formation of PVDF membranes. Desalination 2006, 192 (1-3), 190-197.
49. Bakeri, G.; Matsuura, T.; Ismail, A., The effect of phase inversion promoters on the structure and performance of polyetherimide hollow fiber membrane using in gas–liquid contacting process. Journal of Membrane Science 2011, 383 (1-2), 159-169.
50. Baghbanzadeh, M.; Rana, D.; Lan, C. Q.; Matsuura, T., Effects of inorganic nano-additives on properties and performance of polymeric membranes in water treatment. Separation & Purification Reviews 2016, 45 (2), 141-167.
51. Goh, P.; Ismail, A.; Ng, B., Carbon nanotubes for desalination: Performance evaluation and current hurdles. Desalination 2013, 308, 2-14.
52. Das, R.; Ali, M. E.; Hamid, S. B. A.; Ramakrishna, S.; Chowdhury, Z. Z., Carbon nanotube membranes for water purification: A bright future in water desalination. Desalination 2014, 336, 97-109.
53. Iijima, S., Helical microtubules of graphitic carbon. Nature 1991, 354 (6348), 56.

54. Harris, P. J., Carbon nanotube composites. International Materials Reviews 2004, 49 (1), 31-43.

55. Zhang, Q.; Huang, J. Q.; Qian, W. Z.; Zhang, Y. Y.; Wei, F., The road for nanomaterials industry: A review of carbon nanotube production, post-treatment, and bulk applications for composites and energy storage. Small 2013, 9 (8), 1237-1265.

56. Berber, S.; Kwon, Y.-K.; Tománek, D., Unusually high thermal conductivity of carbon nanotubes. Physical Review Letters 2000, 84 (20), 4613.

57. Hummer, G.; Rasaiah, J. C.; Noworyta, J. P., Water conduction through the hydrophobic channel of a carbon nanotube. Nature 2001, 414 (6860), 188.

58. Kalra, A.; Garde, S.; Hummer, G., Osmotic water transport through carbon nanotube membranes. Proceedings of the National Academy of Sciences 2003, 100 (18), 10175-10180.

59. Striolo, A., The mechanism of water diffusion in narrow carbon nanotubes. Nano Letters 2006, 6 (4), 633-639.

60. Holt, J. K.; Park, H. G.; Wang, Y.; Stadermann, M.; Artyukhin, A. B.; Grigoropoulos, C. P.; Noy, A.; Bakajin, O., Fast mass transport through sub-2-nanometer carbon nanotubes. Science 2006, 312 (5776), 1034-1037.

61. Majumder, M.; Chopra, N.; Andrews, R.; Hinds, B. J., Nanoscale hydrodynamics: enhanced flow in carbon nanotubes. Nature 2005, 438 (7064), 44.

62. Park, J. H.; Sinnott, S. B.; Aluru, N., Ion separation using a Y-junction carbon nanotube. Nanotechnology 2006, 17 (3), 895.

63. Noy, A.; Park, H. G.; Fornasiero, F.; Holt, J. K.; Grigoropoulos, C. P.; Bakajin, O., Nanofluidics in carbon nanotubes. Nano Today 2007, 2 (6), 22-29.

64. Corry, B., Designing carbon nanotube membranes for efficient water desalination. The Journal of Physical Chemistry B 2008, 112 (5), 1427-1434.

65. Song, C.; Corry, B., Intrinsic ion selectivity of narrow hydrophobic pores. The Journal of Physical Chemistry B 2009, 113 (21), 7642-7649.

66. Corry, B., Water and ion transport through functionalised carbon nanotubes: implications for desalination technology. Energy & Environmental Science 2011, 4 (3), 751-759.

67. Fornasiero, F.; Park, H. G.; Holt, J. K.; Stadermann, M.; Grigoropoulos, C. P.; Noy, A.; Bakajin, O., Ion exclusion by sub-2-nm carbon nanotube pores. Proceedings of the National Academy of Sciences 2008, 105 (45), 17250-17255.

68. Coleman, J. N.; Khan, U.; Gun'ko, Y. K., Mechanical reinforcement of polymers using carbon nanotubes. Advanced Materials 2006, 18 (6), 689-706.

69. Sung, J. H.; Kim, H. S.; Jin, H.-J.; Choi, H. J.; Chin, I.-J., Nanofibrous membranes prepared by multiwalled carbon nanotube/poly (methyl methacrylate) composites. Macromolecules 2004, 37 (26), 9899-9902.

70. Wang, X.; Chen, X.; Yoon, K.; Fang, D.; Hsiao, B. S.; Chu, B., High flux filtration medium based on nanofibrous substrate with hydrophilic nanocomposite coating. Environmental Science & Technology 2005, 39 (19), 7684-7691.

71. Chen, W.; Tao, X., Self-organizing alignment of carbon nanotubes in thermoplastic polyurethane. Macromolecular Rapid Communications 2005, 26 (22), 1763-1767.

72. Shawky, H. A.; Chae, S.-R.; Lin, S.; Wiesner, M. R., Synthesis and characterization of a carbon nanotube/polymer nanocomposite membrane for water treatment. Desalination 2011, 272 (1-3), 46-50.

73. Dumée, L.; Sears, K.; Schü tz, J. r.; Finn, N.; Duke, M.; Gray, S., Carbon nanotube based composite membranes for water desalination by membrane distillation. Desalination and Water Treatment 2010, 17 (1-3), 72-79.

74. Dumée, L. F.; Sears, K.; Schütz, J.; Finn, N.; Huynh, C.; Hawkins, S.; Duke, M.; Gray, S., Characterization and evaluation of carbon nanotube Bucky-Paper membranes for direct contact membrane distillation. Journal of Membrane Science 2010, 351 (1-2), 36-43.
75. Dumée, L.; Germain, V.; Sears, K.; Schütz, J.; Finn, N.; Duke, M.; Cerneaux, S.; Cornu, D.; Gray, S., Enhanced durability and hydrophobicity of carbon nanotube bucky paper membranes in membrane distillation. Journal of Membrane Science 2011, 376 (1-2), 241-246.
76. Gethard, K.; Sae-Khow, O.; Mitra, S., Water desalination using carbon-nanotube-enhanced membrane distillation. ACS Applied Materials & Interfaces 2010, 3 (2), 110-114.
77. Bhadra, M.; Roy, S.; Mitra, S., Enhanced desalination using carboxylated carbon nanotube immobilized membranes. Separation and Purification Technology 2013, 120, 373-377.
78. Ragunath, S.; Roy, S.; Mitra, S., Carbon nanotube immobilized membrane with controlled nanotube incorporation via phase inversion polymerization for membrane distillation based desalination. Separation and Purification Technology 2018, 194, 249-255.
79. Tijing, L. D.; Woo, Y. C.; Shim, W.-G.; He, T.; Choi, J.-S.; Kim, S.-H.; Shon, H. K., Superhydrophobic nanofiber membrane containing carbon nanotubes for high-performance direct contact membrane distillation. Journal of Membrane Science 2016, 502, 158-170.
80. Khayet, M.; Matsuura, T., Preparation and characterization of polyvinylidene fluoride membranes for membrane distillation. Industrial & Engineering Chemistry Research 2001, 40 (24), 5710-5718.
81. Tomaszewska, M., Preparation and properties of flat-sheet membranes from poly (vinylidene fluoride) for membrane distillation. Desalination 1996, 104 (1-2), 1-11.

82. Li, Z.; Rana, D.; Wang, Z.; Matsuura, T.; Lan, C. Q., Synergic effects of hydrophilic and hydrophobic nanoparticles on performance of nanocomposite distillation membranes: An experimental and numerical study. Separation and Purification Technology 2018, 202, 45-58.
83. Zhang, J.; Xu, Z.; Shan, M.; Zhou, B.; Li, Y.; Li, B.; Niu, J.; Qian, X., Synergetic effects of oxidized carbon nanotubes and graphene oxide on fouling control and anti-fouling mechanism of polyvinylidene fluoride ultrafiltration membranes. Journal of Membrane Science 2013, 448, 81-92.

3. Effects of multi-walled carbon nanotubes on PVDF nanocomposite membranes for vacuum membrane distillation

Rufan Zhou, Dipak Rana, Takeshi Matsuura, Christopher Q. Lan

Statement of manuscript status and author contribution

A manuscript entitled "Effects of multi-walled carbon nanotubes (MWCNTs) and integrated MWCNTs/SiO_2 nano-additives on PVDF polymeric membranes for vacuum membrane distillation" is currently being prepared based on Chapters 3 and 4 of this thesis.

The roles of the individual researchers are as follows:

- Rufan Z. made project design for Chapters 3 and 4 and performed all the lab work and the data analysis. He also wrote and revised the manuscript of these two chapters.
- Dipak. R. was a project supervisor who provided feedbacks and suggestions on the experiment and data analysis. He also revised the manuscripts.
- Takeshi M. was another supervisor, who provided the feedbacks and suggestions on the experiments, and revised the manuscripts.
- Christopher L. was the primary supervisor, who directed the research. He also helped designing the project, provided feedbacks and suggestions on the experiments, and

revised the manuscripts.

Highlights

- Membranes with MWCNTs additives were fabricated;
- With the MWCNTs addition, the average pore size decreases while the finger-like voids increased.
- Membranes with 2 wt.% of MWCNTs had the maximum membrane vacuum distillation flux.
- MWCNTs did not reinforce the tensile properties of membranes.

Graphical abstract

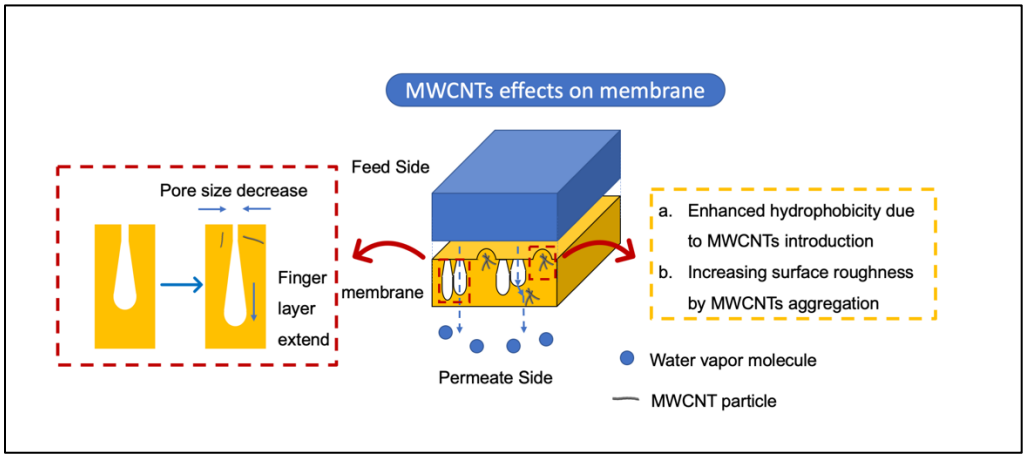

Fig. 3-1 Graphical abstract of MWCNTs effects on membrane

Abstract

Polyvinylidene fluoride (PVDF) was blended with multi-walled carbon nanotubes (MWCNTs) to fabricate nanocomposite vacuum membrane distillation (VMD) membranes

for desalination. Different concentrations (0.5 wt.% - 3 wt.%) of MWCNTs in membrane were tested. It was found that by blending 2 wt.% MWCNTs to PVDF, VMD flux was maximized due primarily to the enlargement and elongation of the finger-like pores, which contributed to the reduction in vapor transport resistance. Extremely high salt rejection (>99.98%) could be maintained by this membrane, while LEPw remained at a reasonably high level (72 psi). Further increase MWCNTs in polymer however led to the deterioration of the membrane performance. The mechanical strength of membrane was considerably weakened upon addition of 1% MWCNTs due to the formation of a large number of macrovoids. However, further increasing of MWCNTs content in the nanocomposite membrane continuously enhanced the membrane's mechanical strength.

Key words

Vacuum membrane distillation, multi-walled carbon nanotubes, PVDF polymeric membrane, membrane structure.

3.1. Introduction

Due to the increasing demand and serious shortage of portable water, more attention has been paid to search for reliable methods and sources to provide freshwater. Water desalination technology, which relies on the abundant seawater and saline water resources, provides a promising prospect for solving the freshwater shortage problems. Typically, the widely accepted desalination technologies are based on thermal processes including multi-stage flash distillation (MSF), and multi-effect distillation (MED) and pressure-driven

membrane separation processes such as reverse osmosis (RO). According to a recent report, these three processes combined contribute to more than 90% of total world installed desalination capacity, among those reverse osmosis (RO) is the most common way of desalination[1].

Membrane distillation (MD) has emerged as an alternative membrane-based technology to produce freshwater. Compared with conventional thermal desalination processes such as MED and MSF, MD could utilize renewable energy such as solar energy for desalination. Compared with conventional RO processes, MD does not require transmembrane pressure difference as the driving force and therefore, consumes less electricity, and is less sensitive to fouling[2-4]. However, commercial application of MD for desalination has been impeded by unsatisfied MD efficiency and long-term durability.

In order to improve the MD membrane performance, some inorganic additives were incorporated into the polymeric matrix of the membrane with successful outcomes[4-5]. Among these additives, carbon nanotubes (CNTs) have attracted a great deal of attention of desalination technology researchers[6-12]. The hydrophobic and atomic scale smooth wall of CNTs' pore provide a rapid transport channel for water molecules[10, 13-15]. Extraordinarily, some CNTs with small channel diameter or special modification could prevent the ions from passing through the channels[16-20]. This unique transport property aroused the enthusiasm of the membrane researchers and many reports on the CNTs based membrane development have appeared in the open literature during the past decade. Moreover, excellent mechanical characteristics of CNTs, which may contribute to

reinforcement of the composite membrane, provide a possible approach for the membrane to resist deterioration after long-term operations[10, 15, 21-22].

One typical approach to use CNTs in MD is immobilizing CNTs in the membrane pores. The membranes fabricated by this method are called carbon nanotubes immobilized membrane (CNIM)[23-24]. CNTs in the pores of polymeric membranes are supposed to contribute to the flux improvement due to the rapid vapor transport through CNTs. In another approach, CNTs are assembled in a paper-like structure, in which CNTs are bound together by Van der Waals force and thus they are allowed to self-support[25-28]. The membrane fabricated by this approach is called Bucky-Paper (BP) membrane. This CNT BP membranes exhibit high hydrophobicity and porosity, both of which are considered as desirable characteristics for the MD membrane.

Despite their promising features, the above two methods suffer from shortcomings that could negatively influence their further applications[29]. In particular, the membrane fabrication by these two approaches are much more complicated compared to the typical membrane fabrication methods. In contrast to the above two methods, blending of CNTs directly into the casting dope seems much simpler and the latter method is indeed effective to enhance the MD performance[29-31]. There are the following advantages of the CNTs blended membrane: 1) Since CNTs are hydrophobic, blending of CNTs enhances the hydrophobicity of the membrane, which is one of the desirable properties of the MD membrane; 2) unlike CNIM, CNTs are anchored firmly to the host polymer matrix by strong interaction forces; 3) unlike BP membrane, CNTs blended membranes are mechanically stable; and 4) CNTs blended membranes are easy to fabricate.

In this work, polyvinylidene fluoride (PVDF) was blended with multi-walled carbon nanotubes (MWCNTs) to prepare nano-composite MD membranes via phase inversion method. The surface and bulk structures of the membranes were investigated by scanning electron microscopy (SEM) and Atomic Force Microscopy (AFM). The membranes were further characterized by measuring the contact angle, liquid entry pressure of water (LEPw) and tensile strength. Finally, the membranes were tested for their VMD performance using either feed distilled water or sodium chloride solution as the feed solutions.

3.2. Experiment

3.2.1. Materials

Polyvinylidene fluoride (PVDF) with different molecular weights, Kynar® HSV740 (Pellet, M_W = 410 kDa) and Kynar® HSV900 (mixture of powders with two molecular weights, Mw_1 = 92,840 kDa and Mw_2 = 1367 kDa), were supplied by Arkema Inc. (Philadelphia, PA, US). Anhydrous N, N-dimethylacetamide (DMAc), which was purchased from Sigma-Aldrich Inc. (St. Louis, MO, US), was used as the solvent for PVDF polymer and to disperse MWCNTs. Pristine MWCNTs (NC7000™ series) prepared by catalytic chemical vapor deposition were supplied by Nanocyl® (Sambreville, Belgium). The average diameter of these MWCNTs is 9.5 nm and the average length is 1.5 μm.

3.2.2. Membrane fabrication

MWCNTs blended membranes with different MWCNTs loadings were fabricated by the phase inversion method. First, an appropriate amount of MWCNTs (0.5 – 3 wt.% to PVDF polymer) was dispersed into 33.5g DMAc with ultrasonication for 30 min (Qsonica Q 700, Newton, CT, US) followed by 1 min vortex mixing. Then, 6 g PVDF (HSV 900: 740 = 2:8) and 0.5g distilled water were added to the MWCNTs/DMAc suspension under continuous stirring at 500 rpm and 60 ºC for 3 h to prepare a uniform casting solution. The ratio of DMAc, PVDF and water is DMAc: PVDF: water = 83.75: 15: 1.25, which is same as the previous work[32-33].

The prepared casting dope solution was degassed under vacuum for 30 min to remove air bubbles before casting on a glass plate by a constant speed automatic film applicator (model AFA-II, Beijing, China). Then, the cast film was immersed into distilled water at room temperature. After peeling off from the glass plate spontaneously the membrane was transferred to another distilled water bath and kept there for 24 h to remove all the residual solvent. The membrane thus formed was taken out of water and then dried at room temperature for 24 h prior to their use.

Membranes were labelled as M-0 or M-Cx, where “M” means membrane, “0” is for pristine PVDF membrane, “C” is for MWCNTs and “x” is the weight percent of MWCNTs in the MWCNTs/PVDF blend (range from 0.5 – 3 wt.% to PVDF polymer).

3.2.3. Membrane characterization

The membrane surface and cross-sectional structure were investigated by Scanning Electron Microscopy (SEM) (JSM-7500F FESEM, JEOL, Japan). The accelerating voltage was 3 kV and the working distance was 10 mm. The pore size of membrane top-surface and the surface porosity were obtained by the ImageJ software from the SEM images of at least 10 random areas. The membrane thickness and finger-layer ratio of membrane were also determined by the ImageJ software.

The roughness of the membrane surface was analyzed by Atomic Force Microscope (AFM) (Park NX10, South Korea). The scan area was 2 μm × 2 μm. The 3D images of membrane top-surface were displayed, and the related surface roughness parameters were obtained by the supporting software.

Water contact angle was measured by the sessile method using the VCA Optima Surface Analysis System (AST Product, Inc. Billerica, MA, US) at room temperature. A 1 μL of deionized water droplet was placed on a dry membrane surface to measure the contact angle. The measurement was repeated at least 10 times at 10 random spots and the average value reported.

The porosity of the membrane was determined by the wet and dry method. A membrane sample was kept immersed in n-butanol for 24 h ensuring the complete wetness of the membrane. After measuring the weight (w_1, g) of the wet sample, it was dried in an oven for 24 h at 50 ºC to make sure the complete evaporation of n-butanol. The dried sample

was measured (w_2, g) and the overall porosity of the membrane was calculated by the equation below:

$$\%\varepsilon = \frac{w_1 - w_2}{A \cdot l \cdot \rho} \times 100\%^{32} \quad (1)$$

Where "ε" means the porosity (%), "A" represents the membrane area (cm^2), "l" indicates the thickness of the samples (cm) and "ρ" is the density of n-butanol (g/cm^3). The average of three samples is reported for each membrane.

The tensile properties of membranes were investigated using the tensile testing instrument (ElectroPuls E3000 Testing Instrument, Instron, Norwood, MA, US) equipped with a 250N load cell. A membrane sample with the size of 4 cm × 2 cm was tested at room temperature. The stretching rate was 5 mm/min and the distance between two grips was 2 cm. The average of three membrane samples is reported.

3.2.4. Liquid entry pressure of water (LEPw) measurement

LEPw indicates the highest pressure applicable without water transfer through the membrane pore, which could quantify the long-term stability of membrane for VMD[31]. It was measured at room temperature by using a static permeation cell. Briefly, a membrane is mounted on a sintered metal plate at the bottom of the feed chamber which is filled with distilled water. Pressure applied from a nitrogen cylinder was increased stepwise by 2 psi every 10 min until the first water droplet appeared at the permeate exit. The pressure was recorded as LEPw. The average of three membrane samples was reported.

3.2.5. Vacuum membrane distillation (VMD)

The performances of all membranes were evaluated by a static VMD setup, the details of which are described in the previous work[32-34]. Briefly, the feed chamber of the setup, which was filled with deionized water or aqueous sodium chloride solution of 35 g/L, could be heated by a heating coil wrapped around the chamber and stirred continuously with a magnetic stirrer. Vacuum of 2.306 kPa was applied to the permeate side and the permeate vapor was collected in a cool trap cooled with liquid nitrogen. The VMD permeated flux was calculated by the equation below:

$$Flux = \frac{w}{t \cdot A}^{32} \quad (2)$$

Where "*w*" is the weight (kg) of condensed permeate vapor collected during the time "*t*" (h) and "*A*" is the effective area of the membrane (0.00113 m^2).

The salt rejection, *%R* was calculated by the equation below:

$$\%R = \frac{C_f - C_p}{C_f} \times 100^{32} \quad (3)$$

"C_f" and "C_p" are, respectively, the conductivity of the feed and condensed permeate measured by a conductivity meter.

3.3. Results and discussion

3.3.1. The effects of MWCNTS on the top surface morphology

Fig. 3-2 shows the top surface SEM image of the membranes with different MWCNTs loadings. The pore size decreased upon loading MWCNTs, which was compatible with data reported earlier[30, 35], but increased with a further increase of MWCNTs loading (Table. 3-1). Table. 3-1 also shows that the surface porosity exhibits an opposite trend.

Table. 3-1 Top-surface characterizations of membranes with different MWCNTs loadings.

Membrane code	Mean pore size (nm)	Maximum pore size (nm)	Minimum pore size (nm)	Surface porosity (%)	Contact angle (degree)
M-0	83.9	140.5	55.8	13.43	81.79(±3.71)
M-C1	71.5	123.2	46.3	13.78	85.04(±2.93)
M-C2	71.8	114.5	49.1	12.22	86.68(±3.00)
M-C3	78.1	128.8	52.1	11.50	84.04(±2.13)

The contact angle increased upon MWCNTs loading as expected from the hydrophobic property of MWCNTs but did not change beyond the error range by further increase in MWCNTs loading.

Fig. 3-3 shows the MWCNTs aggregates, surrounded by circles, at the membrane top surface. The number of aggregates increases with an increase of MWCNTs loading, implying the increase of surface roughness in a typical circumstance[5, 36]. However, the surface roughness decreases in comparison to pristine membranes when MWCNTs are

loaded (Table. 3-2). This suggests that the effect of the decreasing pore size on the surface roughness surpassed the effect of the increase of MWCNTs aggregates. And low interaction tendency among MWCNTs may also result in lower surface roughness.

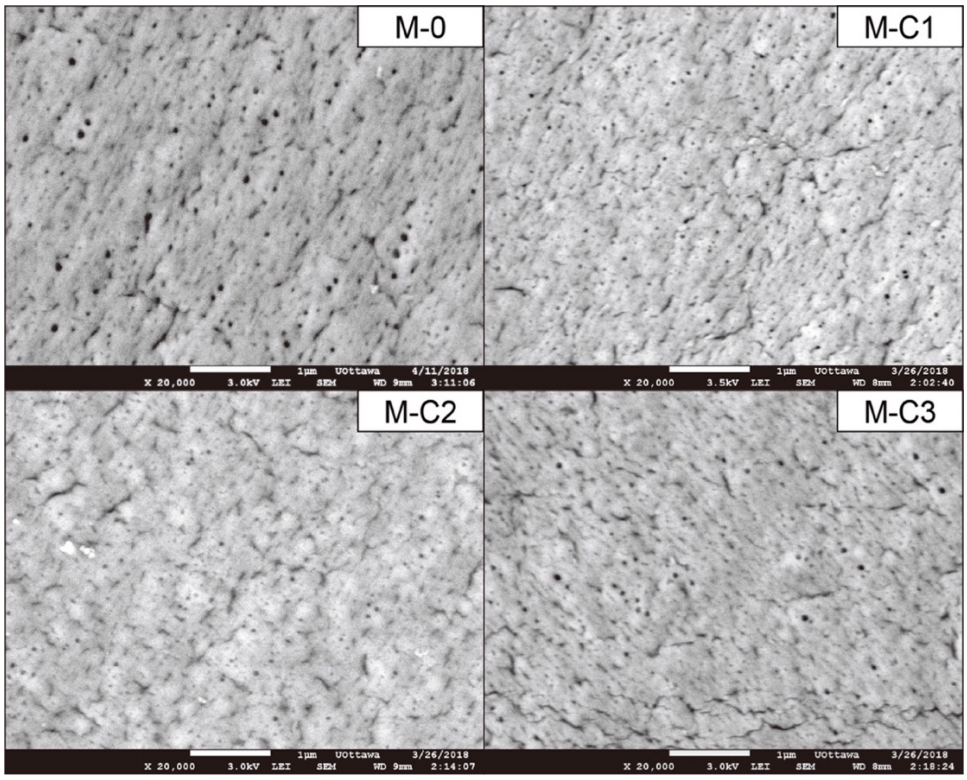

Fig. 3-2 SEM images of the top surface of membranes with different MWCNTs loading loadings.

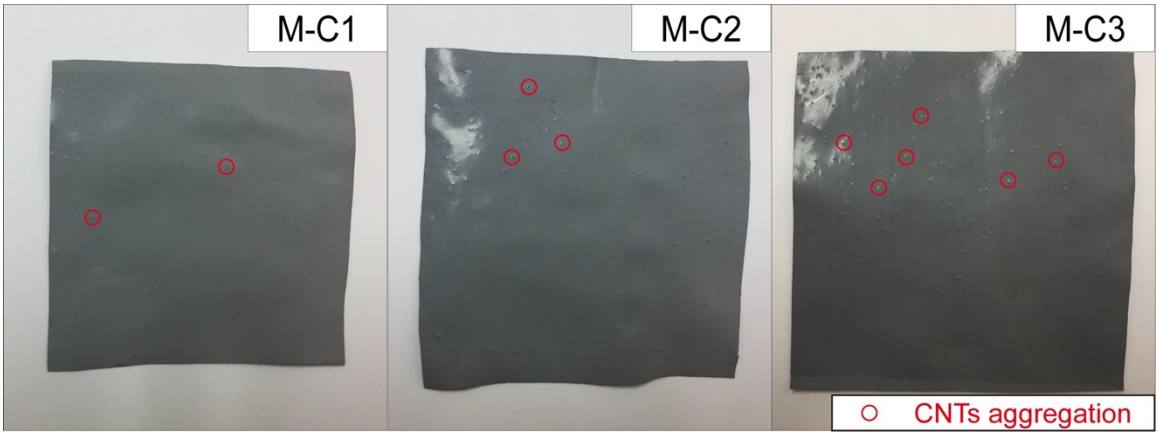

Fig. 3-3 Top surface of membranes with different MWCNTs loadings

Table. 3-2 Comparison of roughness parameter of membrane with/without MWCNTs blending

Membrane Code	R_a (nm)	R_q (nm)	R_{MAX} (nm)
M-0	24.542	29.045	109.100
M-C2	14.260	17.533	79.039

3.3.2. Effects of MWCNTs on cross-sectional structure of membrane

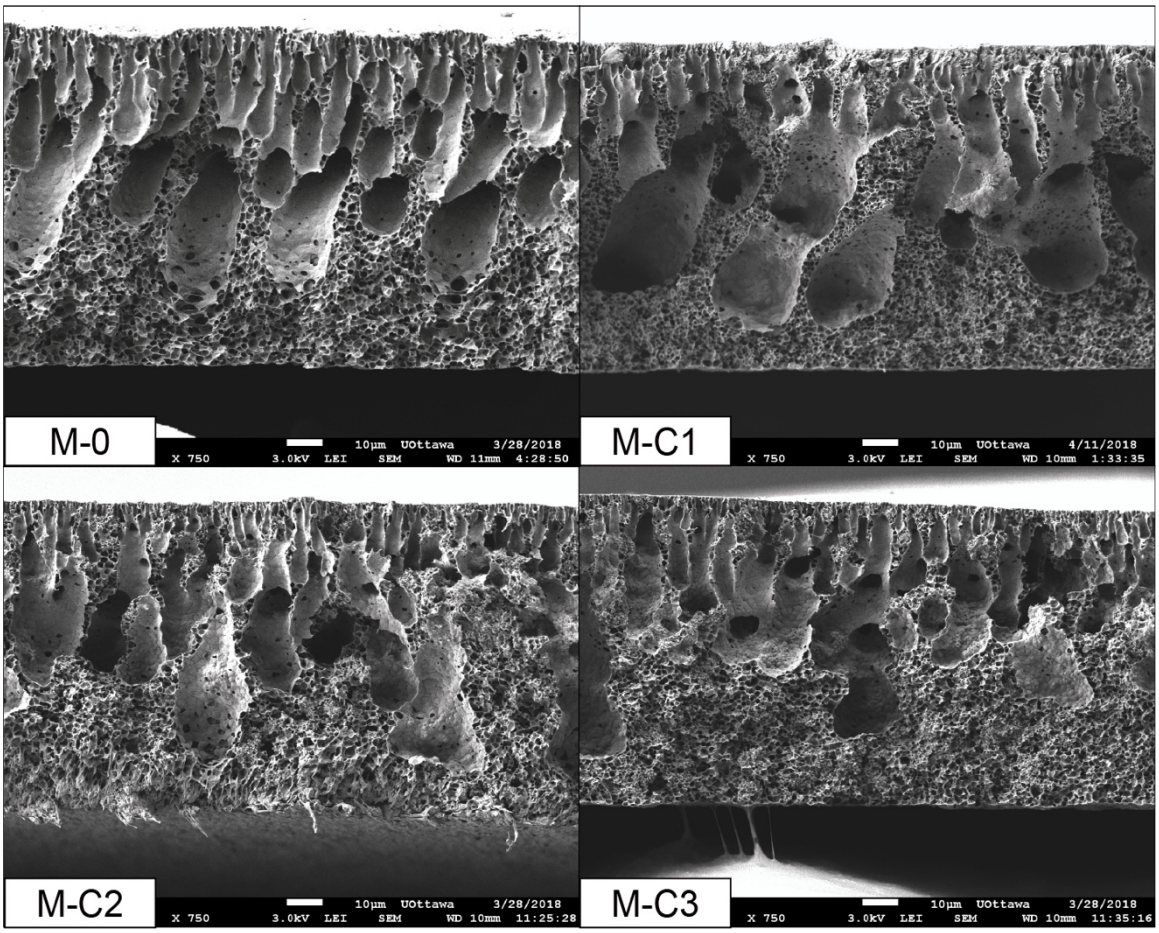

Fig. 3-4 SEM image of cross-sectional area on membranes with different MWCNTs loading ratio.

Fig. 3-4 is the cross-sectional SEM image of the membranes with different MWCNTs loadings. The image exhibits the typical asymmetric structure of polymeric membranes. Upon MWCNTs loading the finger-like macrovoids proceed towards the bottom side of the membrane, however start to recede with a further increase of the MWCNTs loading. As a result, the finger like layer ratio, defined as the thickness of the finger-like layer/the total membrane thickness, shows a maximum at M-C1, which is also reflected in the maximum of membrane porosity at M-C1 and M-C2 (Table 3-3). Another interesting observation is that the pore size of the sponge-like layer decreases by MWCNTs loading. The receding finger-like layer and the densification of the sponge-like layer together result in the decrease in the total membrane thickness with an increase in MWCNTs loading (Table 3-3).

Fig. 3-5 shows the highly magnified SEM images of the sponge- and finger-like layers of the membranes without and with MWCNTs loading. As for the sponge-like layer, aggregates of MWCNTs (shown inside the circle) surrounded by the sponge-like pores are observed in the MWCNTs blended membrane. As well, the pore size of the sponge-like layer is reduced. As for the finger-like layer, pore edges are clearly observed for the membrane without MWCNTs loading. On the other hand, abundant coil like structures, which are likely MWCNTs bundles with sizes of ca 50 nm, are adhering to the pore edges in the MWCNTs blended membrane. However, suggested by other researchers who worked on MWCNT/PVDF polymer, these coil like structures are likely individual MWCNT dispersion wrapped by PVDF polymer[37].

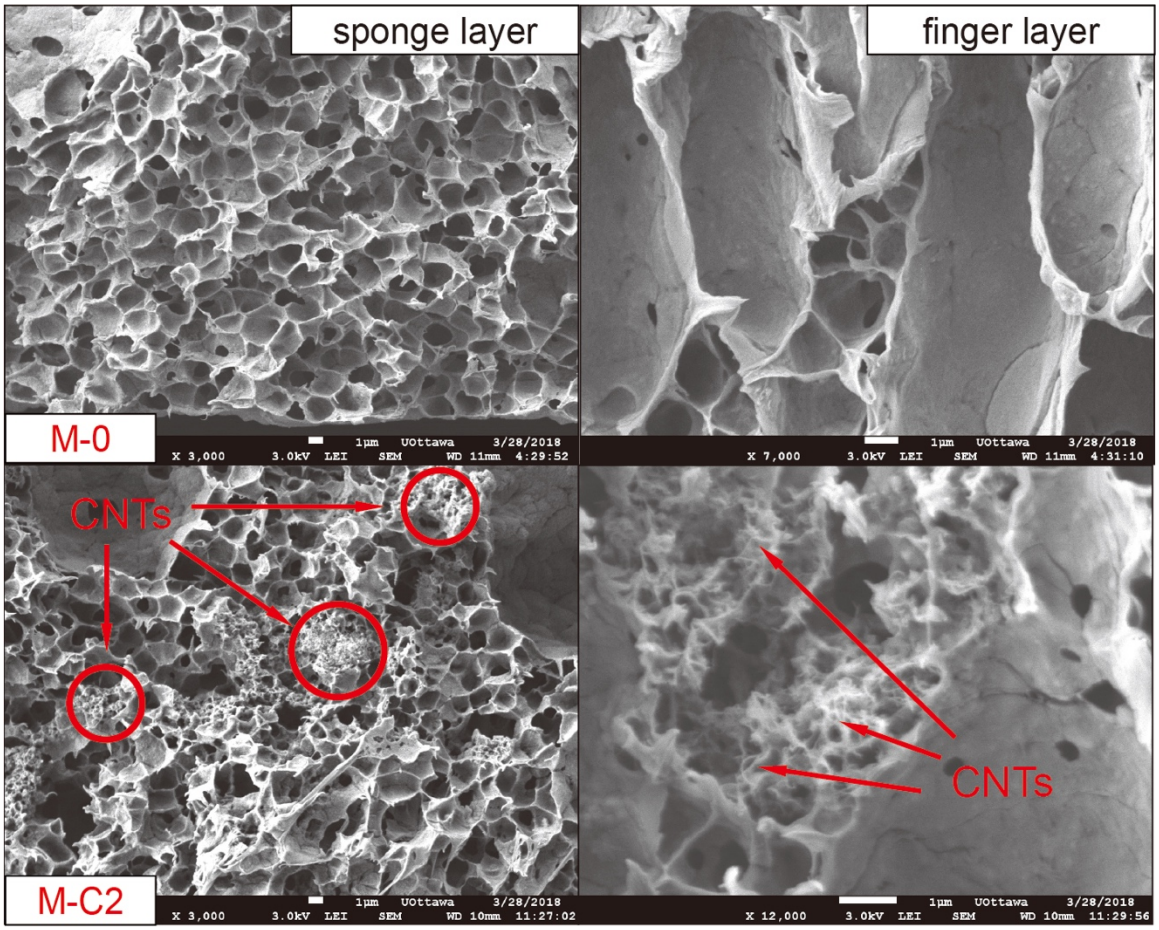

Fig. 3-5 SEM image of different cross-sectional areas on membranes.

Table. 3-3 Some characteristics of membrane with different MWCNTs loadings.

Membrane Code	Thickness (μm)	Finger layer ratio (%)	Porosity (%)
M-0	92.3(±0.4)	64.3(±9.4)	81.16(±0.23)
M-C1	88.1(±0.2)	74.9(±10.8)	85.26(±2.83)
M-C2	85.0(±0.8)	71.2(±11.4)	86.14(±1.70)
M-C3	84.1(±1.1)	64.3(±8.7)	81.00(±1.09)

It is known that the phase inversion rate has a dominant effect on the porous structure of the membrane when the membrane is fabricated by the phase inversion technique[38-41]. Rapid phase inversion would contribute to the formation of finger-like macrovoids,

resulting in membranes of large pore sizes, and high surface as well as overall porosity[40-42]. On the other hand, slow phase inversion would contribute to the formation of sponge-like layer.

The blending of inorganic NPs into casting solution as the nucleating agent facilitates the demixing of polymer-rich and polymer-poor phase and thus the phase inversion[5, 41]. Also, the blending of NPs in the casting solution makes the casting solution thermodynamically less stable, contributing to the fast phase inversion. The blending of the NPs, on the other hand, tends to increase the viscosity of the casting solution, causing the decrease of the demixing rate[39, 43-44]. Therefore, there are two opposing effects of the NPs blending on the phase inversion rate.

The structure of MWCNTs/PVDF blended polymeric composites has attracted much attention because of the blend membrane's promising potential for many applications. The MWCNTs blending into PVDF has a significant effect on the formation of crystalline structure of PVDF. Well-dispersed MWCNTs, as the nucleating agents, could enhance the crystallization rate, contributing to more β-phase formation, which may improve the mechanical property of PVDF polymer[45-46]. On the other hand, according to other researchers, there exists relatively strong interfacial interaction between the MWCNTs and PVDF where the fluorine atoms of PVDF play a connective role[47-48]. Due to this interaction, macromolecules would surround the MWCNTs surface, which may also be a possible reason for the improvement of the mechanical properties of PVDF composites[49]. However, the interaction between the MWCNTs and PVDF impedes the crystal formation

and retards the crystalline rate especially when increasing the MWCNTs content excessively in PVDF polymer[49-51].

As mentioned earlier, the finger layer ratio and the porosity (both surface and overall) show a maximum at M-C1 or M-C2. This can be explained by the two opposing effects of NPs blending on the phase inversion rate. At the low NPs loading, increase in the loading increases the phase inversion rate, leading to the increase in the finger-like layer thickness and the porosity. Beyond M-C1 and M-C2, the increase in the viscosity of the casting solution starts to dominate, leading to the decrease in the finger-like layer thickness and the porosity. As also mentioned earlier, the surface pore size of the membrane shows an opposite trend, i.e. it shows a minimum at M-C1 or M-C2. One possible reason for the decrease of the pore size upon MWCNTs loading is that the strong interaction between the MWCNTs and PVDF impedes the growth of the pore in size. The increase of the pore size beyond M-C2 could be attributed to the severe aggregations of MWCNTs on the membrane surface. The surface pores near the aggregated particles are suggested to exhibit larger pore size according to some researches[52].

As for the surface roughness, the AFM data in Table. 3-2 show a trend opposite to the expectation. It has been demonstrated that the aggregation of inorganic additives on the surface of membrane increased the roughness of membranes[5, 53]. The lowering of roughness upon addition of MWCNTs observed in this work may also be interpreted by the viscosity increase in the presence of MWCNTs in the casting solution. The other reason may be the low interaction tendency between MWCNTs on the surface of membrane which would regularly collocate on the membrane surface like the modified MWCNTs[54].

3.3.3. Tensile property of MWCNTs blended membranes

Table. 3-4 Tensile properties of membranes with different MWCNTs loadings

Membrane Code	Tensile stress at Maximum Load (MPa)	Tensile strain at Break (%)	Young's modulus (MPa)
M-0	2.56(±0.13)	19.69(±1.77)	288.75(±0.75)
M-C1	1.50(±0.01)	16.04(±0.42)	156.21(±1.54)
M-C2	1.91(±0.04)	22.22(±0.23)	207.35(±1.26)
M-C3	2.06(±0.02)	16.67(±0.42)	225.17(±0.88)

Table.3-4 shows the tensile properties of the membranes with different MWCNTs loadings. Both tensile strength at maximum load and the Young's modulus show a dip when 1% MWCNTs was added when compared with that of the pristine membranes. However, both of these two parameters increased when MWCNT content in the nanocomposite membranes increased in the range of 1 to 3%, which is compatible with the previous findings of reasonable increase of the mechanical strength with an increase in the MWCNTs loading[11, 55]. The position of the minimum coincides with those of the maximum finger layer ratio and the overall porosity (M-C1 or M-C2). Hence, it can be concluded that the presence of a large number of the finger-like pores reduces the mechanical strength of the membrane, as reported earlier[56-58]. The increase in PVDF crystallinity and the increase in the interaction at polymer/MWCNTs interfaces can also explain the increase of the tensile strength at higher MWCNTs loadings. However, the poor MWCNTs dispersion and the higher degree of MWCNTs aggregation cannot explain the experimental results since both should reduce the mechanical strength[55, 59]. The tensile strain at the break point behaves in a way different from the tensile stress at maximum load and tensile strain at break.

3.3.4. The VMD performances and LEPw of MWCNTs blended membrane

In Fig. 3-6 LEPw shows a continuous decreasing trend. The decrease in LEPw from M-0 to M-C1 is rather surprizing since pore size decreases while contact angle increases from M-0 to M-C1. The continuous LEPw decrease beyond M-C1 is due to the increase in the surface pore size.

The VMD flux with distilled water feed, also shown in Fig. 3-6, exhibits a maximum at MWCNTs concentration of 2 wt.% (M-C2), which corresponds to more than 100 % increase from the pristine PVDF membrane. Because of this favorable performance, the M-C2 membrane was subjected to VMD experiments with salty feed solution, and the results shown in the Fig. 3-7. The flux decreased during the first 90 min, possibly due to compaction, and later leveled off at 1.64 kg/(m^2·h). The rejection remained above 99.98%. When the feed temperature was increased, the flux reached 5.64 kg/(m^2·h) as shown in Fig. 3-8, while maintaining the high salt rejection.

The position of the maximum VMD flux at M-C1 coincides with the maximum in finger layer ratio and overall porosity (at M-C1 or M-C2), indicating the decrease in the transfer resistance in the finger-like pores contributed to the increase of VMD flux.

Fig. 3-9 summarizes the is the possible impact of MWCNTs loading on the membrane pore structure that causes the change in VMD performance, particularly from M-0 to M-C1. As

shown in the exploded view on the left side of the figure, addition of MWCNTs narrows the surface pore due to the polymer/MWCNTs interfacial interaction, while the accelerated phase inversion makes the finger-like pore wider and longer. As a result, the mass transport resistance decreases, resulting in a significant increase in the vapor flux.

As for the salt reduction, the MWCNTs loading into membrane does not exhibit any negative effect despite the occurrence of MWCNTs aggregation at various parts of the membrane. Some researchers suggest the MWCNTs' introduction into membrane could improve the salt rejection performance as the sorbents[10, 23]. Based on the results from the present and previous works[32, 60] showing above 99.9 % without exception, it seems that the MWCNTs loading has no obvious effect on the salt rejection.

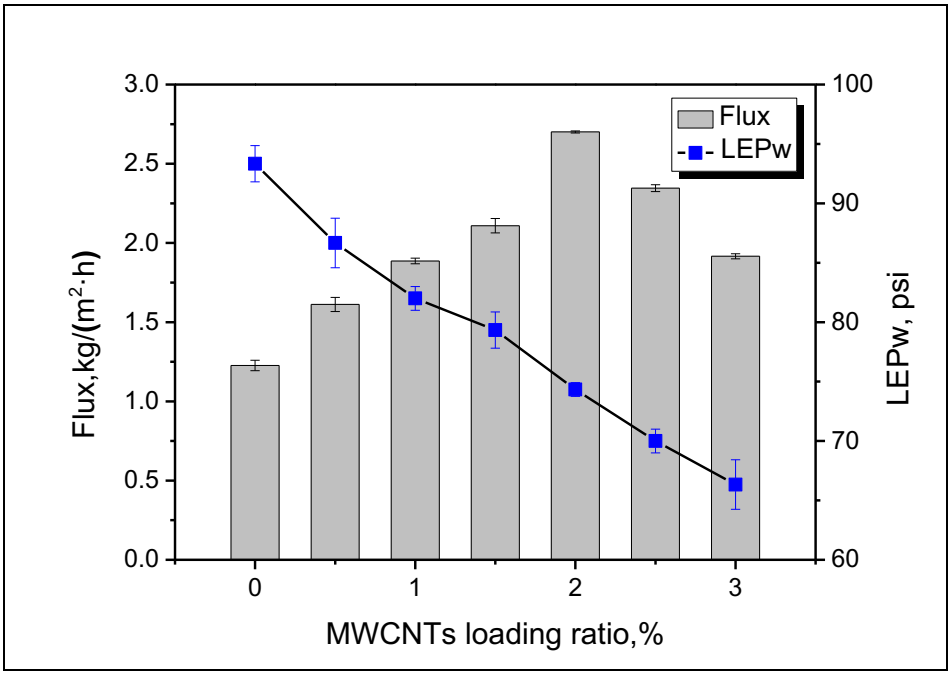

Fig. 3-6 VMD performances and LEPw of membrane with different concentration of MWCNTs

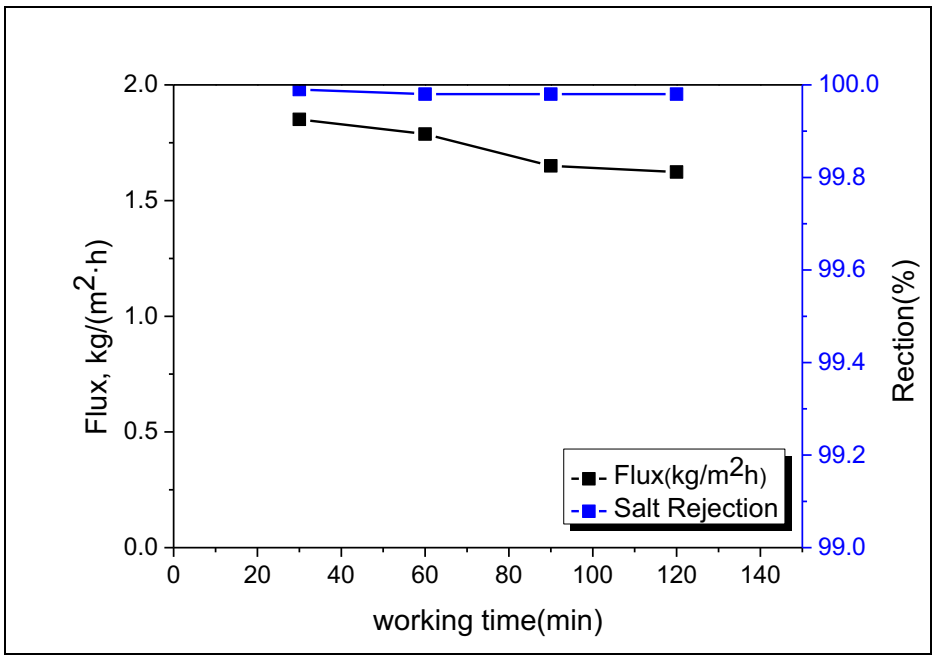

Fig. 3-7 Flux and rejection performance of membrane for long-term operation

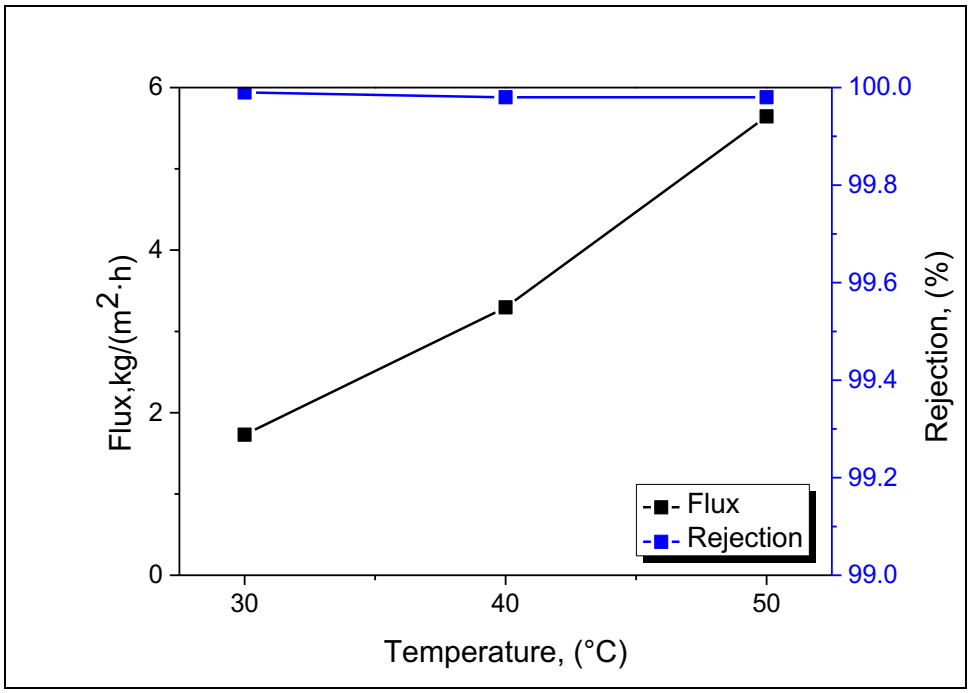

Fig. 3-8 Flux and rejection performance of membrane for different feed side temperature

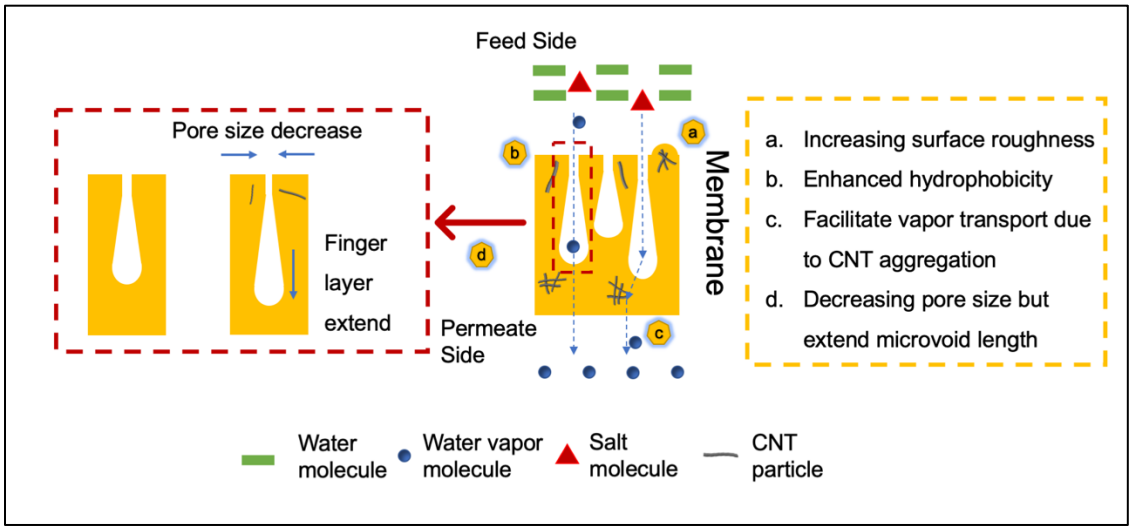

Fig. 3-9 Possible CNT's impacts on membrane structure and vapor permeation

3.3.5. Related researches focusing on CNTs application for desalination by MD

Table. 3-5 summarizes the MD membranes which were fabricated based on carbon nanotubes (CNTs) for desalination. CNTs were incorporated into the membrane either by blending or by immobilizing in the membrane pores. In Bucky-layer membranes CNTs stood alone as mentioned earlier. Compared with the other works, the unique feature of this work is that the membranes were subjected to VMD at relatively low feed temperatures. Therefore, the comparison of desalination performance with the other membranes is difficult. Nevertheless, this work showed one of the highest improvements in flux by CNTs blending with extremely high salt rejections.

Table. 3-5 Comparison of different CNTs applications into MD

Reference	CNT type	Method to prepare membrane	MD configuration	T_{max}[a] on Feed/permeate side	Sea water flux increasing[b] (%)	Maximum salt rejection
		CNT/polymer blended membrane				
[30]	P/F-CNT[c]	Phase inversion	DCMD	82 ºC/20 ºC	~132%	~100%
[29]	P-CNT	Electrospinning	DCMD	60 ºC/20 ºC	~34%	~99.99%
[31]	F-CNT	Electrospinning	DCMD	60 ºC/20 ºC	~43%	~99.98%
This work	P-CNT	Phase inversion	VMD	50 ºC/-	~151%	~99.99%
		Bucky-layer CNT membrane[d]				
[25]	P-CNT	CNT self-supporting BP	DCMD	65 ºC/5 ºC	~ - 400%[e]	~99%
[26]	P-CNT	BP Hot-pressed with support and polymer infiltrated BP	DCMD	95 ºC/5 ºC	~ - 100%	~98.5%
[27]	P/F-CNT	CNT self-supporting BP	DCMD	75 ºC/5 ºC	-	~97%
		CNT Immobilized membrane				
[23]	P-CNT	CNT immobilized on membrane	SGMD hollow fiber	80 ºC/ -	～85%	~15%
[24]	F-CNT	CNT immobilized on membrane	SGMD hollow fiber	90 ºC/ -	~145%	~99%
[62]	P-CNT	CNT immobilized on membrane	DCMD	80 ºC/15-20 ºC	~76%	-

[a] T_{max} is the maximum bulk temperature on feed or permeate side of membrane.

[b] Compared with the artificial sea water (35g/L NaCl solution) flux data of CNTs membranes with non-CNTs membranes from same references.

[c] P indicate pristine and F means functionalize.

[d] The self-supporting BP membrane do not contain any of polymer.

[e] The CNT membrane flux increasing data is comparing with the commercial PTFE membrane from same reference.

3.4. Conclusions

The VMD performance and the other properties of the membranes are well correlated with the membrane morphology; i.e.

1) The VMD flux increases with an increase in the finger-like layer ratio and the overall membrane porosity;
2) The LEPw decreases with an increase in membrane surface pore size (except for the LEPw change caused by the initial 1 wt.% blending of MWCNTs);
3) The mechanical strength of the membrane decreases with an increase in the number and the size of macrovoids.

As a result, the best VMD flux was obtained when 2 wt.% of MWCNTs were blended to PVDF with a flux of 1.64 and 5.6 kg/(m^2·h), respectively, at 30 ºC and 50 ºC of the salty feed solution. The salt rejection of this particular membrane was more than 99.98 % with LEPw 72 psi and the Young's modulus 156.2 MPa. The VMD flux improvement by The VMD flux improvement by MWCNTs blending achieved in this work has surpassed most of the past records on DCMD and SGMD flux improvements caused by the MWCNTs blending.

Reference

1. Burn, S.; Hoang, M.; Zarzo, D.; Olewniak, F.; Campos, E.; Bolto, B.; Barron, O., Desalination techniques—a review of the opportunities for desalination in agriculture. Desalination 2015, 364, 2-16.

2. Lawson, K. W.; Lloyd, D. R., Membrane distillation. Journal of Membrane Science 1997, 124 (1), 1-25.
3. González, D.; Amigo, J.; Suárez, F., Membrane distillation: Perspectives for sustainable and improved desalination. Renewable and Sustainable Energy Reviews 2017, 80, 238-259.
4. Drioli, E.; Ali, A.; Macedonio, F., Membrane distillation: Recent developments and perspectives. Desalination 2015, 356, 56-84.
5. Baghbanzadeh, M.; Rana, D.; Lan, C. Q.; Matsuura, T., Effects of inorganic nano-additives on properties and performance of polymeric membranes in water treatment. Separation & Purification Reviews 2016, 45 (2), 141-167.
6. Hummer, G.; Rasaiah, J. C.; Noworyta, J. P., Water conduction through the hydrophobic channel of a carbon nanotube. Nature 2001, 414 (6860), 188.
7. Kalra, A.; Garde, S.; Hummer, G., Osmotic water transport through carbon nanotube membranes. Proceedings of the National Academy of Sciences 2003, 100 (18), 10175-10180.
8. Kotsalis, E.; Walther, J.; Koumoutsakos, P., Multiphase water flow inside carbon nanotubes. International Journal of Multiphase Flow 2004, 30 (7-8), 995-1010.
9. Holt, J. K.; Park, H. G.; Wang, Y.; Stadermann, M.; Artyukhin, A. B.; Grigoropoulos, C. P.; Noy, A.; Bakajin, O., Fast mass transport through sub-2-nanometer carbon nanotubes. Science 2006, 312 (5776), 1034-1037.
10. Goh, P.; Ismail, A.; Ng, B., Carbon nanotubes for desalination: Performance evaluation and current hurdles. Desalination 2013, 308, 2-14.
11. Coleman, J. N.; Khan, U.; Gun'ko, Y. K., Mechanical reinforcement of polymers using carbon nanotubes. Advanced Materials 2006, 18 (6), 689-706.

12. Wang, L.; Dumont, R. S.; Dickson, J. M., Nonequilibrium molecular dynamics simulation for studying the effect of pressure difference and periodic boundary conditions on water transport through a CNT membrane. Molecular Physics 2017, 115 (8), 981-990.
13. Noy, A.; Park, H. G.; Fornasiero, F.; Holt, J. K.; Grigoropoulos, C. P.; Bakajin, O., Nanofluidics in carbon nanotubes. Nano today 2007, 2 (6), 22-29.
14. Konduri, S.; Tong, H. M.; Chempath, S.; Nair, S., Water in single-walled aluminosilicate nanotubes: Diffusion and adsorption properties. The Journal of Physical Chemistry C 2008, 112 (39), 15367-15374.
15. Ismail, A.; Goh, P.; Sanip, S.; Aziz, M., Transport and separation properties of carbon nanotube-mixed matrix membrane. Separation and Purification Technology 2009, 70 (1), 12-26.
16. Park, J. H.; Sinnott, S. B.; Aluru, N., Ion separation using a Y-junction carbon nanotube. Nanotechnology 2006, 17 (3), 895.
17. Banerjee, S.; Murad, S.; Puri, I. K., Preferential ion and water intake using charged carbon nanotubes. Chemical Physics Letters 2007, 434 (4-6), 292-296.
18. Song, C.; Corry, B., Intrinsic ion selectivity of narrow hydrophobic pores. The Journal of Physical Chemistry B 2009, 113 (21), 7642-7649.
19. Yu, M.; Funke, H. H.; Falconer, J. L.; Noble, R. D., Gated ion transport through dense carbon nanotube membranes. Journal of the American Chemical Society 2010, 132 (24), 8285-8290.
20. Fornasiero, F.; Park, H. G.; Holt, J. K.; Stadermann, M.; Grigoropoulos, C. P.; Noy, A.; Bakajin, O., Ion exclusion by sub-2-nm carbon nanotube pores. Proceedings of the National Academy of Sciences 2008, 105 (45), 17250-17255.

21. Wang, X.; Chen, X.; Yoon, K.; Fang, D.; Hsiao, B. S.; Chu, B., High flux filtration medium based on nanofibrous substrate with hydrophilic nanocomposite coating. Environmental Science & Technology 2005, 39 (19), 7684-7691.
22. Shawky, H. A.; Chae, S.-R.; Lin, S.; Wiesner, M. R., Synthesis and characterization of a carbon nanotube/polymer nanocomposite membrane for water treatment. Desalination 2011, 272 (1-3), 46-50.
23. Gethard, K.; Sae-Khow, O.; Mitra, S., Water desalination using carbon-nanotube-enhanced membrane distillation. ACS Applied Materials & Interfaces 2010, 3 (2), 110-114.
24. Bhadra, M.; Roy, S.; Mitra, S., Enhanced desalination using carboxylated carbon nanotube immobilized membranes. Separation and Purification Technology 2013, 120, 373-377.
25. Dumée, L. F.; Sears, K.; Schütz, J.; Finn, N.; Huynh, C.; Hawkins, S.; Duke, M.; Gray, S., Characterization and evaluation of carbon nanotube Bucky-Paper membranes for direct contact membrane distillation. Journal of Membrane Science 2010, 351 (1-2), 36-43.
26. Dumée, L.; Sears, K.; Schü tz, J. r.; Finn, N.; Duke, M.; Gray, S., Carbon nanotube based composite membranes for water desalination by membrane distillation. Desalination and Water treatment 2010, 17 (1-3), 72-79.
27. Dumée, L.; Germain, V.; Sears, K.; Schütz, J.; Finn, N.; Duke, M.; Cerneaux, S.; Cornu, D.; Gray, S., Enhanced durability and hydrophobicity of carbon nanotube bucky paper membranes in membrane distillation. Journal of Membrane Science 2011, 376 (1-2), 241-246.

28. Morales-Torres, S.; Silva, T. L.; Pastrana-Martínez, L. M.; Brandão, A. T.; Figueiredo, J. L.; Silva, A. M., Modification of the surface chemistry of single-and multi-walled carbon nanotubes by HNO_3 and H_2SO_4 hydrothermal oxidation for application in direct contact membrane distillation. Physical Chemistry Chemical Physics 2014, 16 (24), 12237-12250.
29. Tijing, L. D.; Woo, Y. C.; Shim, W.-G.; He, T.; Choi, J.-S.; Kim, S.-H.; Shon, H. K., Superhydrophobic nanofiber membrane containing carbon nanotubes for high-performance direct contact membrane distillation. Journal of Membrane Science 2016, 502, 158-170.
30. Silva, T. L.; Morales-Torres, S.; Figueiredo, J. L.; Silva, A. M., Multi-walled carbon nanotube/PVDF blended membranes with sponge-and finger-like pores for direct contact membrane distillation. Desalination 2015, 357, 233-245.
31. An, A. K.; Lee, E.-J.; Guo, J.; Jeong, S.; Lee, J.-G.; Ghaffour, N., Enhanced vapor transport in membrane distillation via functionalized carbon nanotubes anchored into electrospun nanofibres. Scientific Reports 2017, 7, 41562.
32. Efome, J. E.; Baghbanzadeh, M.; Rana, D.; Matsuura, T.; Lan, C. Q., Effects of superhydrophobic SiO_2 nanoparticles on the performance of PVDF flat sheet membranes for vacuum membrane distillation. Desalination 2015, 373, 47-57.
33. Baghbanzadeh, M.; Rana, D.; Lan, C. Q.; Matsuura, T., Effects of hydrophilic silica nanoparticles and backing material in improving the structure and performance of VMD PVDF membranes. Separation and Purification Technology 2016, 157, 60-71.
34. Chen, Z.; Rana, D.; Matsuura, T.; Yang, Y.; Lan, C. Q., Study on the structure and vacuum membrane distillation performance of PVDF composite membranes: I. Influence of blending. Separation and Purification Technology 2014, 133, 303-312.

35. Zhang, J.; Xu, Z.; Shan, M.; Zhou, B.; Li, Y.; Li, B.; Niu, J.; Qian, X., Synergetic effects of oxidized carbon nanotubes and graphene oxide on fouling control and anti-fouling mechanism of polyvinylidene fluoride ultrafiltration membranes. Journal of Membrane Science 2013, 448, 81-92.
36. Niksefat, N.; Jahanshahi, M.; Rahimpour, A., The effect of SiO2 nanoparticles on morphology and performance of thin film composite membranes for forward osmosis application. Desalination 2014, 343, 140-146.
37. Yuan, J.-K.; Yao, S.-H.; Dang, Z.-M.; Sylvestre, A.; Genestoux, M.; Bai1, J., Giant dielectric permittivity nanocomposites: realizing true potential of pristine carbon nanotubes in polyvinylidene fluoride matrix through an enhanced interfacial interaction. The Journal of Physical Chemistry C 2011, 115 (13), 5515-5521.
38. Van de Witte, P.; Dijkstra, P. J.; Van den Berg, J.; Feijen, J., Phase separation processes in polymer solutions in relation to membrane formation. Journal of Membrane Science 1996, 117 (1-2), 1-31.
39. Fontananova, E.; Jansen, J. C.; Cristiano, A.; Curcio, E.; Drioli, E., Effect of additives in the casting solution on the formation of PVDF membranes. Desalination 2006, 192 (1-3), 190-197.
40. Bakeri, G.; Matsuura, T.; Ismail, A., The effect of phase inversion promoters on the structure and performance of polyetherimide hollow fiber membrane using in gas–liquid contacting process. Journal of Membrane Science 2011, 383 (1-2), 159-169.
41. Hou, D.; Dai, G.; Fan, H.; Wang, J.; Zhao, C.; Huang, H., Effects of calcium carbonate nano-particles on the properties of PVDF/nonwoven fabric flat-sheet composite membranes for direct contact membrane distillation. Desalination 2014, 347, 25-33.

42. Kim, J.-H.; Lee, K.-H., Effect of PEG additive on membrane formation by phase inversion. Journal of Membrane Science 1998, 138 (2), 153-163.

43. Celik, E.; Park, H.; Choi, H.; Choi, H., Carbon nanotube blended polyethersulfone membranes for fouling control in water treatment. Water Research 2011, 45 (1), 274-282.

44. Emadzadeh, D.; Lau, W.; Matsuura, T.; Ismail, A.; Rahbari-Sisakht, M., Synthesis and characterization of thin film nanocomposite forward osmosis membrane with hydrophilic nanocomposite support to reduce internal concentration polarization. Journal of Membrane Science 2014, 449, 74-85.

45. Lee, J. S.; Kim, G. H.; Kim, W. N.; Oh, K. H.; Kim, H. T.; Hwang, S. S.; Hong, S. M., Crystal structure and ferroelectric properties of poly (vinylidene fluoride)-carbon nano tube nanocomposite film. Molecular Crystals and Liquid Crystals 2008, 491 (1), 247-254.

46. Kim, G. H.; Hong, S. M.; Seo, Y., Piezoelectric properties of poly (vinylidene fluoride) and carbon nanotube blends: β-phase development. Physical Chemistry Chemical Physics 2009, 11 (44), 10506-10512.

47. Chen, G.-X.; Li, Y.; Shimizu, H., Ultrahigh-shear processing for the preparation of polymer/carbon nanotube composites. Carbon 2007, 45 (12), 2334-2340.

48. Owens, F. J.; Jayakody, J.; Greenbaum, S. G., Characterization of single walled carbon nanotube: Polyvinylene difluoride composites. Composites Science and Technology 2006, 66 (10), 1280-1284.

49. Almasri, A.; Ounaies, Z.; Kim, Y. S.; Grunlan, J., Characterization of solution-processed double-walled carbon nanotube/poly (vinylidene fluoride) nanocomposites. Macromolecular Materials and Engineering 2008, 293 (2), 123-131.

50. Ke, K.; Wang, Y.; Yang, W.; Xie, B.-H.; Yang, M.-B., Crystallization and reinforcement of poly (vinylidene fluoride) nanocomposites: Role of high molecular weight resin and carbon nanotubes. Polymer Testing 2012, 31 (1), 117-126.
51. He, L.; Xu, Q.; Hua, C.; Song, R., Effect of multi-walled carbon nanotubes on crystallization, thermal, and mechanical properties of poly (vinylidene fluoride). Polymer Composites 2010, 31 (5), 921-927.
52. Yang, Y.; Zhang, H.; Wang, P.; Zheng, Q.; Li, J., The influence of nano-sized TiO_2 fillers on the morphologies and properties of PSF UF membrane. Journal of Membrane Science 2007, 288 (1-2), 231-238.
53. Zhang, L.; Shi, G.-Z.; Qiu, S.; Cheng, L.-H.; Chen, H.-L., Preparation of high-flux thin film nanocomposite reverse osmosis membranes by incorporating functionalized multi-walled carbon nanotubes. Desalination and Water Treatment 2011, 34 (1-3), 19-24.
54. Vatanpour, V.; Madaeni, S. S.; Moradian, R.; Zinadini, S.; Astinchap, B., Fabrication and characterization of novel antifouling nanofiltration membrane prepared from oxidized multiwalled carbon nanotube/polyethersulfone nanocomposite. Journal of Membrane Science 2011, 375 (1-2), 284-294.
55. Moniruzzaman, M.; Winey, K. I., Polymer nanocomposites containing carbon nanotubes. Macromolecules 2006, 39 (16), 5194-5205.
56. Shi, L.; Wang, R.; Cao, Y.; Feng, C.; Liang, D. T.; Tay, J. H., Fabrication of poly (vinylidene fluoride-co-hexafluropropylene)(PVDF-HFP) asymmetric microporous hollow fiber membranes. Journal of Membrane Science 2007, 305 (1-2), 215-225.

57. Lai, C. Y.; Groth, A.; Gray, S.; Duke, M., Enhanced abrasion resistant PVDF/nanoclay hollow fibre composite membranes for water treatment. Journal of Membrane Science 2014, 449, 146-157.

58. Sukitpaneenit, P.; Chung, T.-S., Molecular elucidation of morphology and mechanical properties of PVDF hollow fiber membranes from aspects of phase inversion, crystallization and rheology. Journal of Membrane Science 2009, 340 (1-2), 192-205.

59. Xie, X.-L.; Mai, Y.-W.; Zhou, X.-P., Dispersion and alignment of carbon nanotubes in polymer matrix: A review. Materials Science and Engineering: R: Reports 2005, 49 (4), 89-112.

60. Baghbanzadeh, M.; Hirceaga, N.; Rana, D.; Matsuura, T.; Lan, C. Q., Effects of Polymer Ratio and Film-Penetration Time on the Properties and Performance of Nanocomposite PVDF Membranes in Membrane Distillation. Industrial & Engineering Chemistry Research 2016, 55 (37), 9971-9982.

61. Koo, J. W.; Han, J. H.; Lee, S. H.; Sohn, J. S.; Choi, J. S. In Development of Nano-carbon bucky-paper membranes for membrane distillation, Materials Science Forum, Trans Tech Publ: 2012; pp 408-411.

62. Ragunath, S.; Roy, S.; Mitra, S., Carbon nanotube immobilized membrane with controlled nanotube incorporation via phase inversion polymerization for membrane distillation based desalination. Separation and Purification Technology 2018, 194, 249-255.

4. Hybrid SiO_2/multi-walled carbon nanotubes (MWCNTs) nanocomposite PVDF membranes for vacuum membrane distillation

Rufan Zhou, Dipak Rana, Takeshi Matsuura, Christopher Q. Lan

Highlights

- Hybrid nanocomposite membranes with additives MWCNTs and SiO_2 were fabricated;
- Hybrid nanocomposite membranes with 1% SiO_2, integrated additive shows synergetic effects on vapor flux through membrane;
- High SiO_2 content could increase LEPw of membrane compared with membrane blended MWCNTs only;
- MWCNTs exhibits different effects on tensile properties of membrane when loading ratio of SiO_2 is different.

Graphical abstract

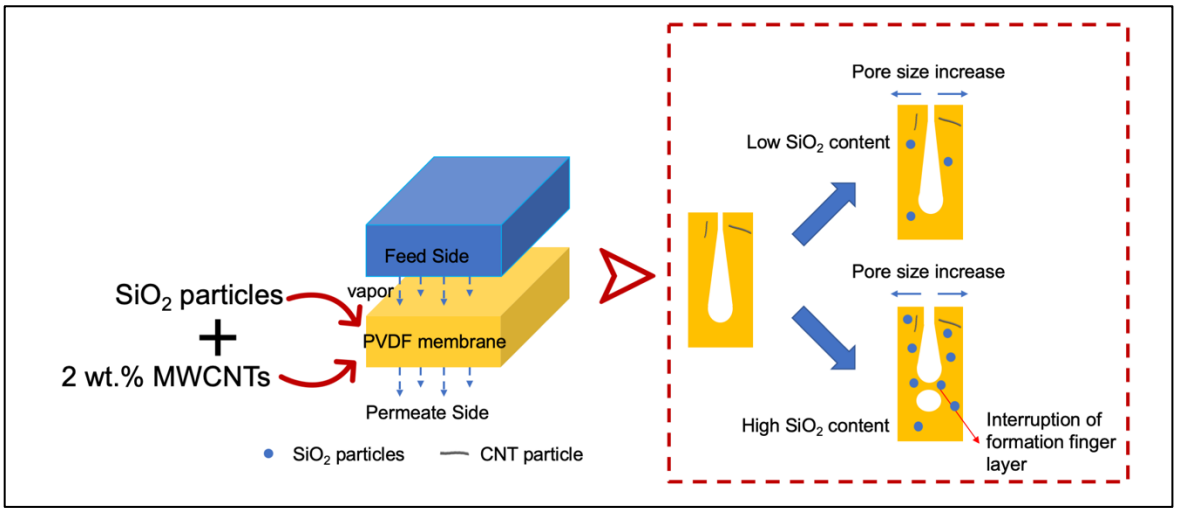

Fig. 4-1 Possible mechanism of integrated additives loaded on membrane

Abstract

One of three different SiO_2 nanoparticles (NPs) (hydrophobic, superhydrophobic and hydrophilic) was added with multi-walled carbon nanotubes (MWCNTs) to dope solution to fabricate hybrid PVDF nanocomposite membranes by the phase inversion technique. Integration of MWCNTs with low content SiO_2 NPs was proven to have synergistic effects on the improvement of VMD flux due to the increase of overall porosity by MWCNTs and growth of the macrovoids by SiO_2 NPs. Especially, MWCNTs played a dominant role at low SiO_2 NPs content. Compared with the pristine PVDF membrane and the nanocomposite PVDF membrane with MWCNTs additives in chapter 3, respectively, the flux of the membrane with the integrated additives increased by 292 % and 55 %. On the other hand, SiO_2 NPs, at their high content, start to dominate the effect on the membrane performance. In particular, at high SiO_2 NPs contents, the asymmetric structure of PVDF

membrane disappeared, leading to low mechanical strength. All fabricated membranes exhibit great desalination potential with salt rejection as high as >99.97%.

Key words

Vacuum membrane distillation, multi-walled carbon nanotubes, hybrid nanocomposite membrane, PVDF polymeric membrane.

4.1. Introduction

As a significant challenge in the past few decades, freshwater scarcity has been threatening to the public health, food production, industrial efficiency and environment sustainability. Membrane distillation (MD), an emerging desalination technology employing seawater and brackish water, has attracted great attention due to its unique benefits, such as high salt rejection, low energy consumption, etc.[1-3]. The porous membrane, whose structure and properties strongly influence the performance and productivity of desalination, plays a crucial role in membrane distillation. In order to improve the membrane performance in MD, different membrane fabrication and modification methods have been proposed and their effectiveness has been studied[1, 4-5].

As a valid modification approach, the incorporation of nano-additives directly into polymeric membranes exhibits great potentials in enhancing the performance of membrane distillation. Of particular relevance, different kinds of nano-additives have been investigated on their effectiveness to improve the porosity, hydrophobicity, pore size and

other critical membrane properties[6-9]. Among these additives, CNTs have a promising future in MD application due to their specific hollow structures and superior durability[5, 10-13]. Three major methods to utilize CNTs to fabricate membranes for membrane distillation (carbon nanotube immobilized membrane (CNIM), CNTs self-supporting bucky-paper (BP) membrane and CNTs blended membrane) have proved the feasibility of CNTs in membrane modification[8, 13-15]. In particular, the CNTs blended membrane, as the simplest CNTs utilizing method, exhibited excellent MD performance and extraordinary mechanical intensity[8, 13, 16]. In chapter 3, addition of appropriate amount of introduced MWCNTs (2 wt.% to polymer which is 0.3 wt. % to casting dope) could enhance the VMD vapor flux with little decrease of LEPw. However, comparing with other additives, e.g. CuO and hydrophilic SiO_2, the improvement of membrane performance by CNTs loading was not necessarily remarkable[4,9].

SiO_2 nanoparticles (NPs), as nano-fillers into the membrane, have demonstrated their capacity to dramatically enhance the MD flux[7,9]. However, mechanical strength is weakened[17-19] and LEPw (liquid entry pressure of water) is lowered[7, 9] when the content of SiO_2 NPs is very high (which could even reach 50 % to the polymer), which would have negative effects on the long term stability of the membrane[13, 20]. Therefore, reinforcement additives, such as MWCNTs, are expected to increase the mechanical properties of membrane when loaded with SiO_2 NPs. On related notes, CNTs hybrid nano-fillers have been demonstrated their benefit to the performance of nanocomposites. For example, CNTs and graphene have proven to have synergetic effects to improve the mechanical and electrical properties of polymer composites due to the integrated net structure protecting the CNTs damage[21-23]. And also, in similar studies, integrated nano-additives of graphene

oxide and CNTs demonstrated the effectiveness of the method to improve ultrafiltration performance[24]. Hence, it is reasonable to expect that the addition of CNTs, as an enhancer of the mechanical strength, combined with SiO_2 NPs, would likely to exhibit a synergistic effect leading to the fabrication of a high flux membrane with better mechanical strength and therefore long durability.

Hence, integral nano-fillers based on the combination of CNTs and SiO_2 nanoparticles seem worth studying. In this work, pristine multi-walled CNTs (MWCNTs) and different kinds of SiO_2 NPs were blended with polyvinylidene fluoride (PVDF) polymers to prepare hybrid nanocomposite membranes via the phase inversion method. All of these membranes were tested in VMD of distilled and artificial salty water, and the membranes are characterized by various methods to have a better understanding of the roles of MWCNTs and SiO_2 NPs to membrane structure and performance.

4.2. Experiment

4.2.1. Materials

Polyvinylidene fluoride (PVDF) of two different molecular weights, Kynar® HSV740 (Pellet, MW = 410 kDa) and Kynar® HSV900 (mixture of powders with two molecular weight, Mw_1 = 92,840 kDa and Mw_2 = 1367 kDa), were kindly supplied by Arkema Inc. (Philadelphia, PA, US). Anhydrous N, N-dimethylacetamide (DMAc) purchased from Sigma-Aldrich Inc. (St. Louis, MO, US) was used as the solvent to dissolve PVDF polymer. Pristine MWCNTs, NC7000™ series prepared by Catalytic Chemical Vapor

Deposition (CCVD) process, was obtained from Nanocyl® (Sambreville, Belgium). The average diameter of these MWCNTs was 9.5 nm and average length 1.5 μm. All SiO_2 nanoparticles were purchased from Skyspring Nanomaterials Inc. (Houston, TX, US) and their sizes and modification methods are summarized in Table. 4-1.

Table. 4-1 Properties of NPs supplied by the manufactures.

SiO_2 type	Average particle size (From product data)	Particles size (Measured using TEM)	Modification method
Hydrophobic	10-20 nm	15.16(±0.688) nm	single layer organic chain
Super-hydrophobic	10-25 nm	20.54(±0.992) nm	single layer organic chain
Hydrophilic	10-20 nm	33.87(±1.042) nm	amino group

4.2.2. Membrane fabrication

All membranes were fabricated by the phase inversion method. Firstly, 2 wt.% MWCNTs (to PVDF polymer which equals to 0.3 wt.% to casting solution) were dispersed into 33.5g DMAC with ultrasonication for 30 min (Qsonica Q 700, Newton, CT, US) followed by 1 min vortex mixing. Then, 6g of PVDF (HSV 900: 740 = 2:8) and 0.5g of distilled water were added to MWCNTs/DMAC suspension prepared above under continuous stirring at 500 rpm and 60 ºC for 3 h to ensure uniformity of the casting dope. The ratio of water, PVDF and DMAC solution was the same as our previous work focusing on the effects of SiO_2 on MD membrane performance[7, 9].

After the preparation of MWCNTs/PVDF blend casting dope, a predetermined amount of silicon dioxide particles (1 wt.% and 7 wt.% to the total casting dope) were added to the dope and the mixture was kept stirred for 2 h at room temperature, before it was degassed for 30 min under vacuum to remove air bubbles. The casting dope so prepared was cast on a glass plate using a uniform-speed automatic film applicator (model AFA-II, Beijing, China), followed by immersion of the cast film into distilled water at room temperature. When the membrane peeled off from the glass plate spontaneously, it was transferred to another distilled water bath and kept there for 24 h to remove the residual solvent. The, the membrane was dried at room temperature for one day.

All the membranes in the present work were labelled as M-0 or M-CxNy. “M-0” means pristine PVDF membrane; In M-C2Ny, “C” indicates MWCNTs, M-C2 was the membrane with best VMD flux in chapter 3. “N” is either “B” (hydrophobic SiO_2) or “S” (super-hydrophobic SiO_2) or “L” (hydrophilic SiO_2) and the “y” indicates the content of N in the casting dope (1 wt.% and 7 wt.% in the total casting dope).

4.2.3. Membrane characterization

The top surface and the cross-sectional structure were investigated by Scanning Electron Microscopy (SEM) (JSM-7500F FESEM, JEOL, Japan) under 3 kV accelerating voltage and 10 mm working distance. The pore size of membrane top-surface and surface porosity were obtained by the ImageJ software based on the SEM images of at least ten random areas. Cross-sectional images were also analyzed by the ImageJ software to evaluate the finger-like layer ratio and the membrane thickness.

Atomic Force Microscope (AFM) (Park NX10, South Korea) was used to analyze the surface roughness of the fabricated membranes with 2 μm × 2 μm scan area and the related roughness parameters were obtained via the supported software.

The hydrophobicity of the membrane top-surface was evaluated by water contact angle measurement by VCA Optima Surface Analysis System (AST Product, Inc. Billerica, MA, US). Around 1 μL of deionized water was dropped on the dry surface of membrane and the contact angle was measured at room temperature at ten random spots. The measurement was repeated at least 10 times and the average value was reported.

The porosity of membrane was determined by the wet and dry method. Three samples were cut from different areas of a membrane and kept immersed in n-butanol for 24 h to ensure complete wetting of the samples. The weight (w_1, g) of the wet sample was measured, followed by drying in an oven for 24 h at 50 ºC to make sure complete evaporation of n-butanol. The weight (w_2, g) of the dry sample was then measured. The porosity of membrane was calculated by the equation below:

$$\%\varepsilon = \frac{w_1 - w_2}{A \cdot l \cdot \rho} \times 100\%^{7} \quad (1)$$

Where "ε" is the porosity (%), "A" is the membrane sample's area (cm^2), "l" is the thickness of the samples (cm), and "ρ" is the density of n-butanol (g/cm^3). The average of the three samples was reported.

The tensile properties of the membranes were evaluated by Tensile Testing Instrument (ElectroPuls E3000 Testing instrument, Instron, Norwood, MA, US) loaded with 250 N.

The size of the measured samples was 4 cm × 2 cm and the tests were carried out at room temperature. The stretching rate was 5 mm/min and the distance between two grips was 2 cm. Three samples were taken from each membrane and average values reported.

4.2.4. Particles characterization and aggregation analysis

The SiO_2 NPs were subjected to the Transmission Electron Microscopy (TEM) (FEI Tecnai G2 Spirit Twin TEM) after dispersing the particles in methanol by sonication for 10 min. The TEM images were analyzed by the ImageJ software to obtain the particle sizes.

The MWCNTs and PVDF polymer aggregation was investigated by phase-contrast microscope (Infinity II BX40, Olympus, Canada) at 20×, 200× and 400× magnification. The samples for the microscope were prepared by mixing 0.5 g of the casting dope with 9.5g DMAc by ultrasonication for 30 min, followed by 1 min vortex mixing. Then, 1.5 μL of the sample was dropped on the microscope slide, which was then covered with a microscope cover glass. The size of the aggregates was measured by analyzing the microscopic images using the ImageJ software.

4.2.5. Liquid entry pressure of water (LEPw) measurement

The liquid entry pressure of water (LEPw) is the minimum transmembrane pressure required for distilled water to permeate through the membrane pores, quantifying its long-term operation stability[13, 20]. LEPw was measured using a conventional static permeation cell. The membrane sample was placed on a sintered metal plate located at the bottom of

the permeation cell and below the feed chamber that was filled with distilled water. Pressure applied to the feed chamber from a nitrogen cylinder was increased stepwise by 2 psi every 10 minutes. The LEPw value was recorded as the pressure value at which the first water droplet appeared at the permeate exit. Three samples were taken from each membrane, and the average value recorded.

4.2.6. Vacuum membrane distillation (VMD)

The membrane distillation performance of all the membranes fabricated in the present work was evaluated by a static VMD setup, the details of which were described in the previous works[7, 9, 25]. Briefly, the setup is a batch system consisting of a static permeation cell wrapped with heating coil, two cold traps and a vacuum pump (Fig. 4-2). A membrane sample is placed at the bottom of the permeation cell and below the feed chamber that is filled with either distilled water or aqueous NaCl solution of 35 g/L. The feed liquid was stirred continuously with a stirrer to prevent the temperature and concentration polarization. Vacuum of 2.306 kPa was applied to the permeate side of the membrane via a vacuum pump. The permeate vapor was collected in the cool trap cooled with liquid nitrogen. The VMD flux was calculated by the equation below:

$$Flux = \frac{w}{t \cdot A}{}^{7} \quad (2)$$

Where "*w*" (kg) is the weight of condensed vapor collected in the cold trap during time "*t*" (h) and "*A*" is the effective area of the membrane sample (0.00113 m^2).

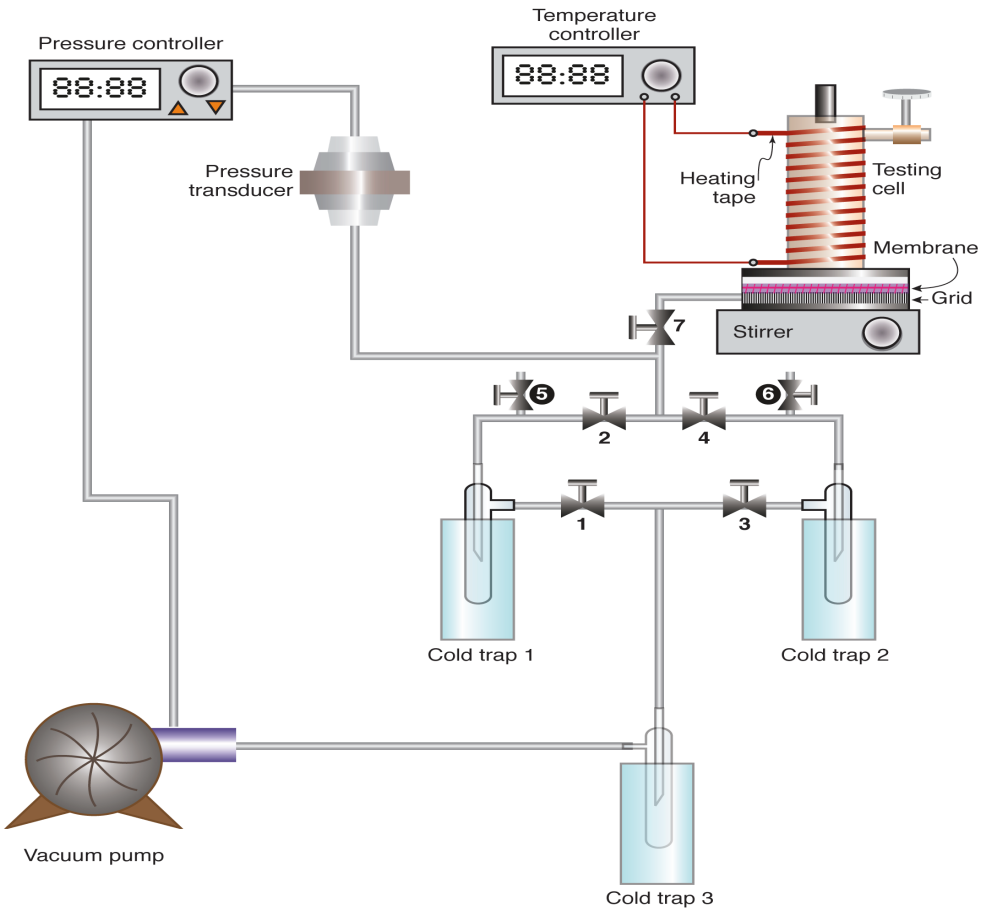

Fig. 4-2 Schematic illustration of VMD setup[25]

The rejection of membrane was calculated by the equation below:

$$\%R = \frac{C_f - C_p}{C_f} \times 100^7 \quad (3)$$

Where "R" means the rejection, "C_f" and "C_p" are the conductivity of the feed and the condensed vapor, respectively, measured by a conductivity meter (OAKTON, CON 2700). Every measurement was carried out when the flux became stable several hours after the VMP experiment was begun.

4.3. Results and discussion

4.3.1. Hybrid nanocomposite membranes with low SiO_2 NPs content (1%)

Table. 4-2 Top-surface characterizations of membranes.

Membrane code	Mean pore size (nm)	Maximum pore size (nm)	Minimum pore size (nm)	Surface porosity (%)	Contact angle (degree)
Nanocomposite membrane with MWCNTs only					
M-C2	71.8	114.5	49.1	12.22	86.68(±3.00)
Nanocomposite membrane with SiO2 particles only					
M-L7	78.0	130.1	50.1	11.77	81.25(±1.36)
Hybrid nanocomposite membrane with low SiO_2 content					
M-C2B1	76.6	128.6	50.5	16.12	84.69(±1.90)
M-C2S1	76.8	119.9	45.1	15.50	87.50(±1.36)
M-C2L1	76.8	132.8	47.9	16.02	86.39(±1.14)
Hybrid nanocomposite membrane with high SiO_2 content					
M-C2B7	86.7	168.7	53.4	11.61	88.50(±1.56)
M-C2S7	96.8	178.9	53.1	12.08	91.61(±2.14)
M-C2L7	79.5	130.4	43.0	15.57	84.23(±1.28)
M-C8L7	74.4	126.0	47.2	13.30	83.67 (±2.13)

It was reported in Chapter 3 that M-C2 (2 wt.% of MWCNTs blend to PVDF polymer which is 0.3 wt.% to casting dope) exhibited the highest VMP flux among all the membranes studied in Chapter 3. Besides, M-C2 demonstrated much larger mechanical strength than M-C1, the nanocomposite membrane blended with 1% MWCNTs. Hence M-C2 was chosen as the control membrane to which various amounts of different SiO_2 NPs

were added to know the effects of SiO_2 NPs addition on the membrane properties and the membrane's VMD performance.

Table. 4-3 Thickness, finger layer ratio and porosity of membranes

Membrane Code	Thickness (μm)	Finger layer ratio (%)	Porosity (%)
Nanocomposite membrane with MWCNTs only			
M-C2	85.0(±0.8)	71.2(±11.4)	86.14(±1.70)
Nanocomposite membrane with SiO_2 particles only			
M-B1	-[a]	-	79.87(±1.14)
M-S1	-	-	81.77(±1.41)
M-L1	-	-	80.25(±2.60)
M-B7	-	-	71.37(±1.04)
M-S7	-	-	72.59(±1.99)
M-L7	111.3(±0.5)	76.4(±13.5)	71.93(±3.77)
Hybrid nanocomposite membrane with low SiO_2 content			
M-C2B1	78.5(±0.9)	63.0(±9.7)	84.39(±1.02)
M-C2S1	90.6(±0.3)	71.2(±11.4)	82.85(±5.43)
M-C2L1	84.9(±0.6)	67.6(±14.1)	84.32(±5.62)
Hybrid nanocomposite membrane with high SiO_2 content			
M-C2B7	94.0(±0.7)	59.1(±5.7)	70.77(±2.18)
M-C2S7	146.5(±0.3)	60.4(±10.1)	71.96(±0.39)
M-C2L7	112.9(±0.8)	80.5(±11.7)	67.36(±2.13)
M-C8L7	146.0(±0.6)	-[b]	65.36(±4.01)

[a]: The thickness and finger-like layer ratio were not measured.

[b]: There's no obvious finger like pores on membrane.

Fig. 4-3 shows the SEM images of top surface of all the membranes listed in Table 4-2 except for M-C2. Table. 4-2 summarizes the data related to the porous structure of the membrane surface and the contact angle. Comparing M-C2 and M-C2N1 (N means the

nanoparticles), where NP is either B or S or L, it is found that, with 1 wt.% adding of different SiO_2 NPs, the mean pore size and surface porosity increase considerably without much change in contact angle. As well, the differences among different NPs are small.

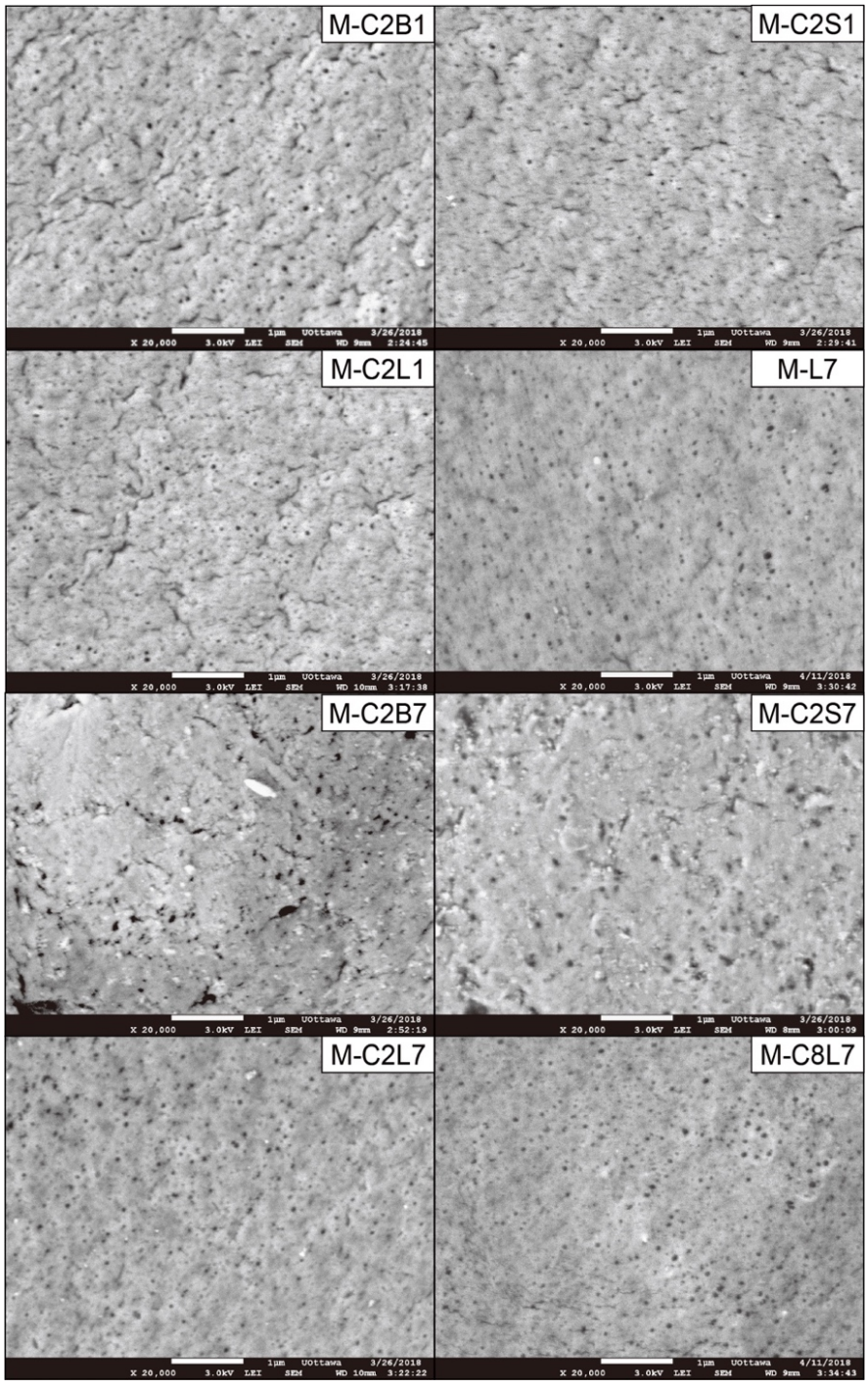

Fig. 4-3 SEM image of top surface of membranes listed in Table 4-2.

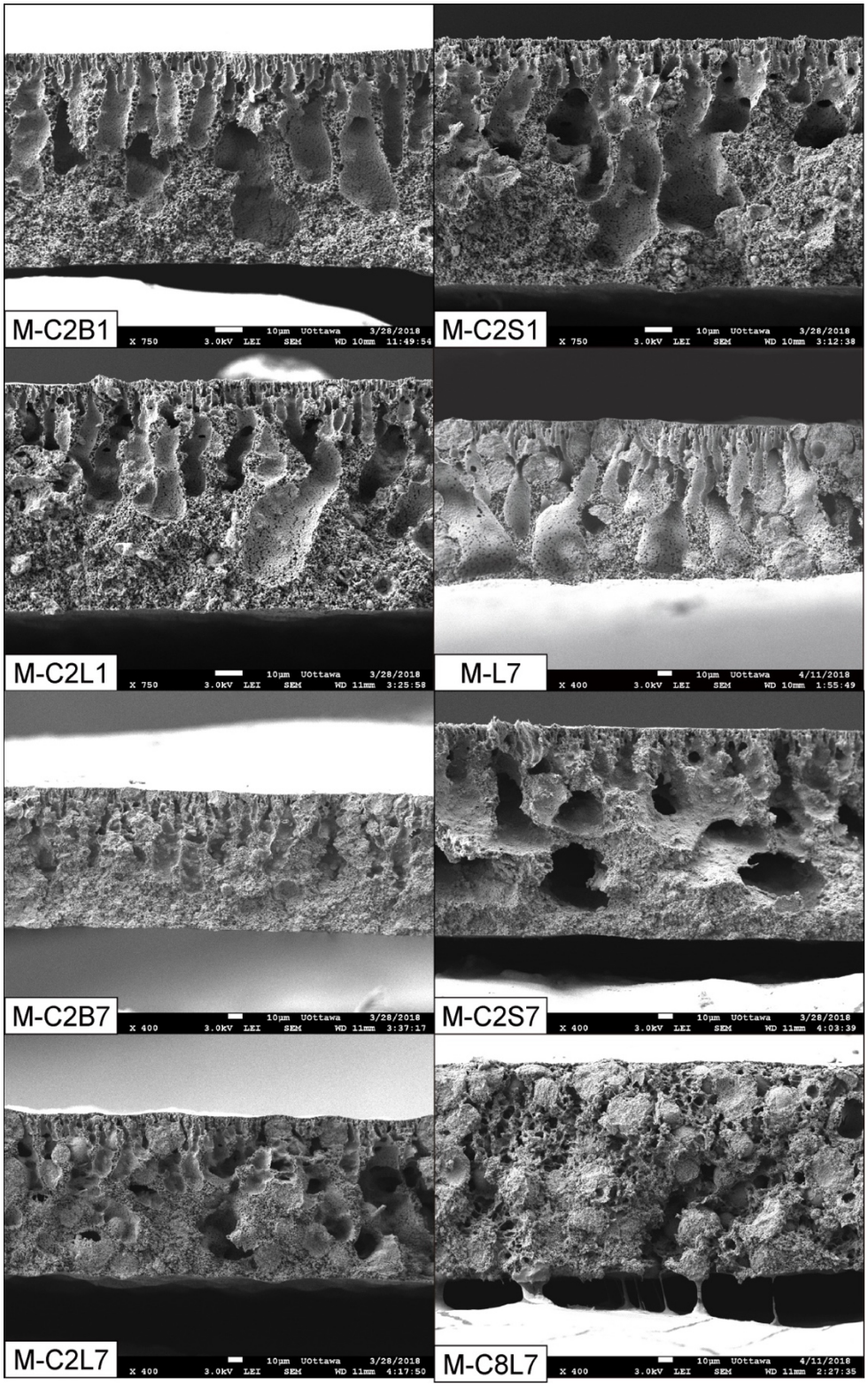

Fig. 4-4 SEM cross-sectional images of the membranes listed in Table. 4-2.

Table. 4-4 Tensile properties of membranes with different MWCNTs loadings

Membrane Code	Tensile stress at Maximum Load (MPa)	Tensile strain at Break (%)	Young's modulus (MPa)
Nanocomposite membrane with MWCNTs only			
M-C2	1.91(±0.04)	22.22(±0.23)	207.35(±1.26)
Nanocomposite membrane with SiO_2 particles only			
M-B1	1.77(±0.10)	19.12(±0.27)	219.35(±0.16)
M-S1	1.34(±0.03)	18.75(±0.21)	140.18(±0.52)
M-L1	1.61(±0.01)	20.48(±0.60)	184.31(±0.93)
M-B7	0.70(±0.03)	8.06(±0.58)	146.06(±0.53)
M-S7	0.47(±0.03)	9.79(±0.07)	60.28(±1.40)
M-L7	1.01(±0.02)	6.29(±0.04)	124.45(±1.67)
Hybrid nanocomposite membrane with low SiO_2 content			
M-C2B1	1.60(±0.12)	12.71(±1.04)	217.46(±2.24)
M-C2S1	1.04(±0.06)	11.93(±0.80)	139.65(±3.50)
M-C2L1	1.51(±0.00)	15.52(±0.90)	181.40(±1.69)
Hybrid nanocomposite membrane with high SiO_2 content			
M-C2B7	0.95(±0.04)	8.58(±0.54)	150.88(±0.91)
M-C2S7	0.49(±0.01)	12.82(±0.48)	67.30(±0.80)
M-C2L7	0.92(±0.01)	6.36(±0.07)	127.38(±0.40)
M-C8L7	0.95(±0.03)	3.16(±0.46)	177.24(±1.43)

Remembering that the surface pore size and surface porosity decreased upon loading of MWCNTs alone (Chapter 3), due to the MWCNTs/PVDF interactions, the addition of N, either B or S or L, impeded the above interactions, thus resulted in the increase in the surface pore size and surface porosity. Another possible explanation for the increase in surface pore size is the better dispersion of MWCNTs as SiO_2 NPs are added.

The cross-sectional SEM images of membranes listed in Table 4-2 (except for M-C2) are shown in Fig. 4-4 and the results of the ImageJ analysis are given in Table. 4-3. The latter table also includes the data for NPs loading without MWCNTs. In Fig. 4-4, all membranes with low SiO_2 NPs content exhibit the typical asymmetric membrane structure. In Table 4-3, compared with M-C2, the overall porosity and finger layer ratio of M-C2N1 (N=B and L) decrease, which may be attributed to the further delayed demixing caused by the increase in dope viscosity when SiO_2 NPs are added. The decrease in finger layer ratio and the overall porosity will have negative effects on the VMD flux due to the increase in the mass transfer resistance.

Table 4.4. shows the tensile properties of the membrane. Comparing M-C2 and M-C2N1 (N=B and L), tensile properties decreased with 1% addition of SiO_2 NPs. As revealed in Chapter 3, membrane porosity is correlated with the VMD performance and mechanical properties of membrane[4, 20, 26-27]. Typically, membrane with higher overall porosity resulting from more finger-like macrovoids formation shows weaker tensile properties[26, 28]. Unexpectedly, the mechanical properties were reduced by SiO_2 NPs addition, despite the decrease in overall porosity. The possible reason is that the adding of SiO_2 NPs impedes the interaction between MWCNTs and PVDF, thus lowering the tensile properties. Comparing M-N1 and M2C1, the tensile properties were reduced by MWCNTs introduction, with porosity increased.

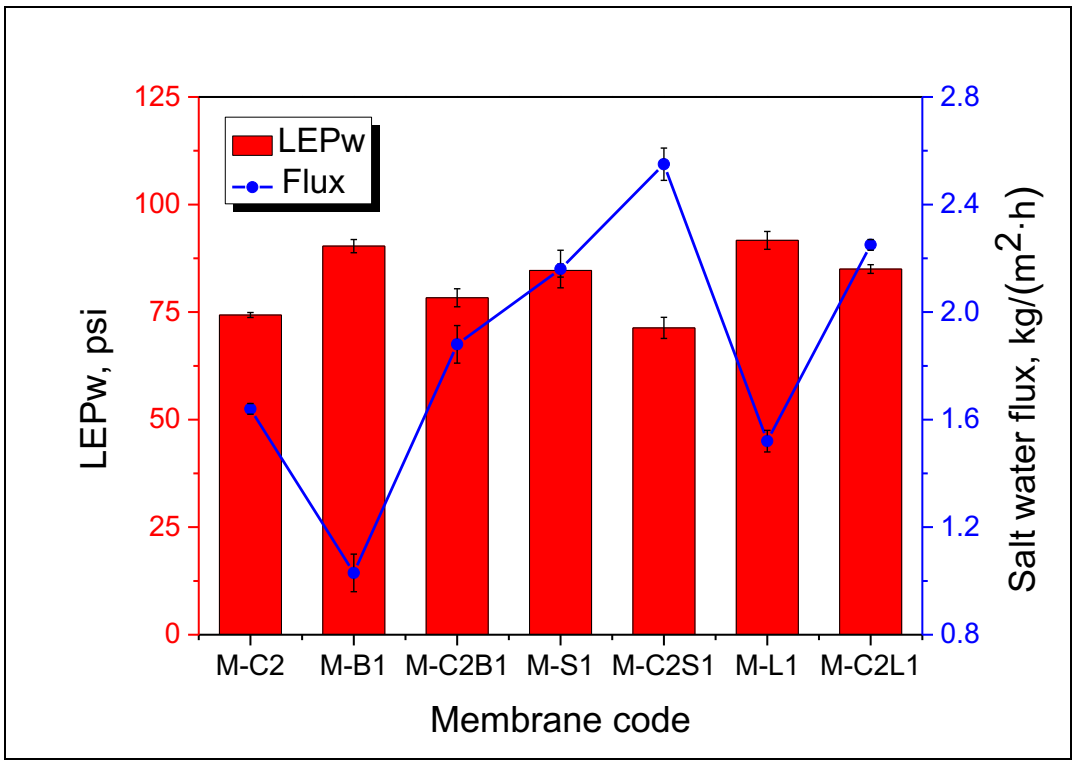

Fig. 4-5 VMD performance and LEPw of hybrid nanocomposite membranes (low SiO2 content)

Fig. 4-5 shows the VMD performance with the salty feed and LEPw of the M-C2N1(N1 is 1 wt. % SiO_2 NPs blended) membrane together with those of M-C2 and M-N1 membrane. First, comparing M-C2 with M-N1, the flux of M-N1 (N=B) is lower than, higher than (N=S) or nearly equal to (N=L) M-C2, despite the fact M-N1's overall porosity is always lower than M-C2 (Table 4-3). Then, comparing M-N1 and M-C2N1, flux of M-C2N1 is higher than M-N1, regardless of N = B, S, L. In other words, addition of MWCNTs to the SiO_2 NPs increased the flux without exception. This can be explained by the higher overall porosity of M-C2N1 than M-N1 (Table 4-3). Further, comparing M-C2 with M-C2N1, the flux of the latter membrane is higher than the former without exception. In summary, addition of SiO_2 NPs individually does not necessarily result in the flux increase from M-C2, but their addition together with MWCNTs enhances the VMD flux remarkably. As a

result, M-C2S1 exhibited the highest flux of 2.5 kg/(m^2·h) in the presence of salt in the feed.

4.3.2. Hybrid nanocomposite membranes with high SiO_2 NPs content (7 %)

Fig. 4-3 also includes the top surface SEM of M-C2N7, where 7 wt.% SiO_2 NPs was added together with MWCNTs loading. The reason for the choice of 7 wt.% SiO_2 NPs is that an optimal VMD performance was achieved in the earlier work[7, 9]. At this dope composition, the weight ratio of SiO_2 NPs and MWCNTs is 28:1.2. Table 4-2 also include the data for M-C2N7. According to the table, the surface pore size increases M-C2B1 to MC2-B7 and M-C2S1 to M-C2S7, while the maximum and minimum pore size decrease from M-C2L1 to M-C2L7. Surface porosity decreases from M-C2N1 to M-C2N7, regardless of hydrophobic or hydrophilic property of N. As for contact angle, it increases from M-C2B1 to M-C2B7 and M-C2S1 to M-C2S7, while decreases from M-C2L1 to MC2-L7, which is natural since B and S are hydrophobic while L is hydrophilic.

Fig. 4-4 also includes the cross-sectional image of M-C2N7 and the results of their ImageJ analysis are given in Table. 4-3. In Fig. 4-4, as SiO_2 NPs content increases from 1 to 7%, the asymmetric structure of membrane disappears, and the presence of macrovoids dominates especially for M-C2S7 and M-C2L7. In Table. 4-3 the membrane thickness increases from M-C2N1 to M-C2N7, while the overall porosity decreases from M-C2N1 to M-C2N7. As for finger layer ratio, it decreases for B and S but increases for L, which agrees with the general trends, i.e. hydrophobic additive discourages the formation of

finger-like pore[6-7], whereas hydrophilic additive encourages the formation of finger-like pore[9, 29].

Fig.4-3 and Table 4-2 also include M-C8L7. Compared with M-C2L7, mean pore size and surface porosity decrease, and contact angle change is within the error range. The cross-sectional image of M-C8L7 in Fig. 4-4 no longer exhibits an asymmetric structure and, correspondingly, the overall porosity was the lowest among all prepared membranes. Hence, at the SiO_2 NPs content as high as 7%, the property of SiO_2 start to govern the cross-sectional morphology of the membrane, while the excessive amount of MWCNTs has only negative effect on the membrane morphology.

Table. 4-5 shows the roughness data of hydrophilic SiO_2 (L) membranes with different MWCNTs loadings. The roughness decreases upon loading of MWCNTs from M-L7 to M-C2L7. This is similar to the roughness decrease from M-0 to M-C2, which is ascribed to the MWCNTs interaction. However, with the further increase in MWCNTs loading to M-C2L7, the roughness increases due to the formation of many swells at the membrane surface caused by the MWCNTs aggregates.

Table. 4-4 summarizes the tensile properties of the M-C2N7 membranes. Comparing M-C2N1 and M-C2N7, all tensile properties are less for M-C2N7 despite the decrease in overall porosity (Table 4-3). This is because of the size of the macrovoids and disappearance of the asymmetric structure of the membrane as shown in Fig. 4-4. Comparing M-N7 with M-C2N7, MWCNTs could enhance the tensile properties of membrane corresponding to slight decrease of overall porosity of membranes. With further

increase of MWCNTs in M-C8L7, the asymmetric structure totally disappears and only macrovoids are observed. So, the tensile strain at break of M-C8L7 was the lowest on among these membranes.

Table. 4-5 Surface roughness parameters of L7 membranes.

Membrane Code	R_a (nm)	R_q (nm)	R_{MAX} (nm)
M-L7	27.587	32.008	98.944
M-C2L7	12.084	15.646	67.978
M-C8L7	110.732	122.916	343.920

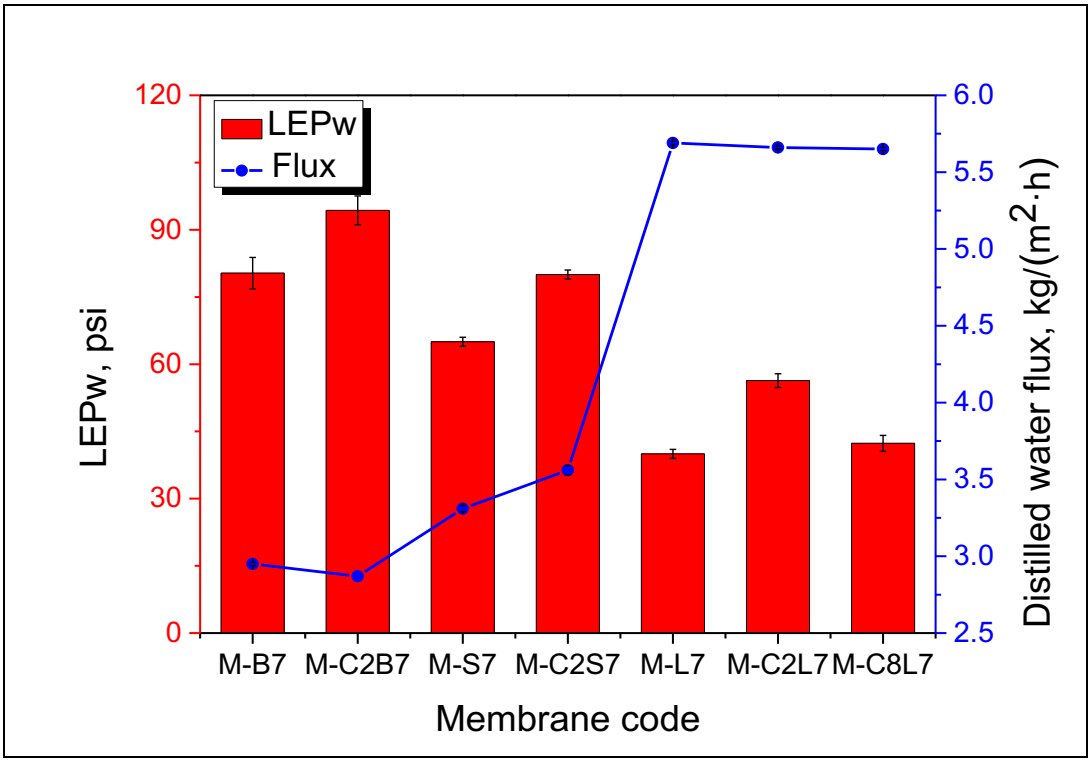

Fig. 4-6 Pure water VMD performance and LEPw for hybrid nanocomposite membranes with high SiO_2 content (7%)

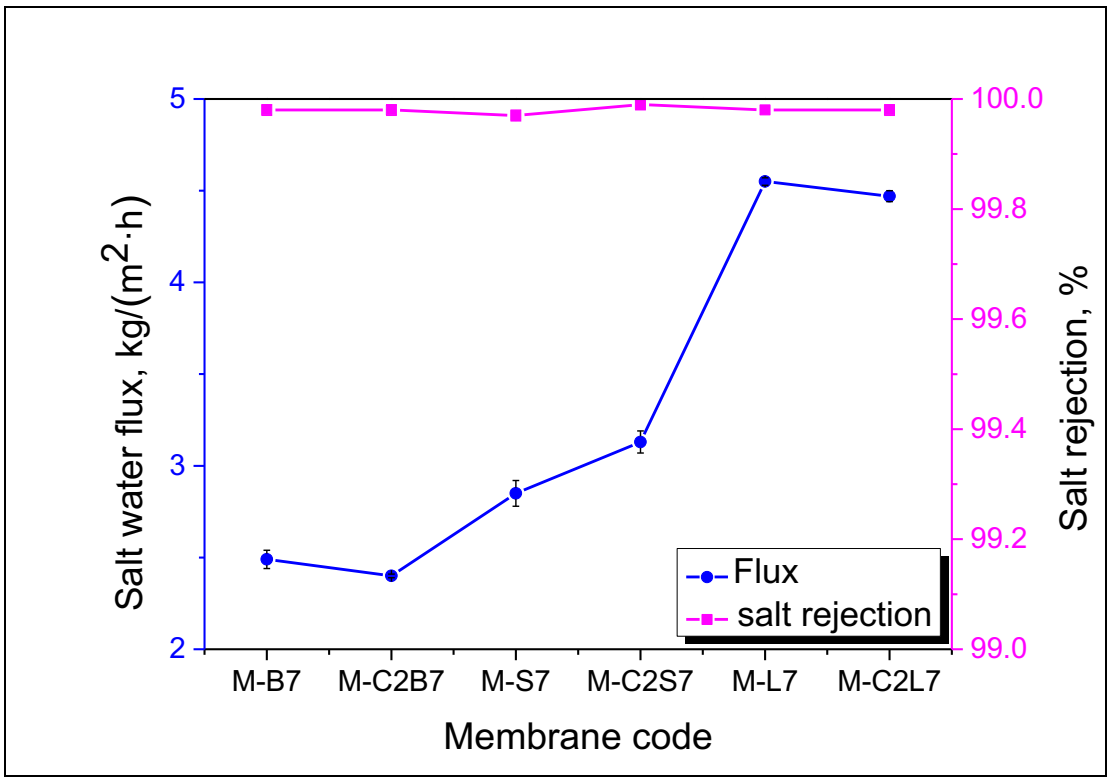

Fig. 4-7 Salty water VMD performance for for hybrid nanocomposite membranes with high SiO_2 content (7%)

Fig. 4-6 shows vapor flux when the feed is distilled water and LEPw for the M-N7 and M-C2N7 membranes and Fig. 4-7 shows the vapor flux when the feed is the salty water and the salt rejection. In Fig. 4-6, LEPw increases from M-N7 to M-C2N7. The flux decreases for B, increases for S and nearly the same for L. M-L7, in which there are many large macrovoids (Fig. 4-4), shows very high pure water flux and the loading of MWCNTa do not have much effect. As a result, M-L7, M-C2L7 and M-C8L7 all show the highest but similar pure water fluxes of 5.7 kg/(m^2h). The flux data with the salty feed solution given in Fig. 4-7 parallel the pure water permeation fluxes given in Fig. 4-6, except that the fluxes in Fig. 4-7 are lower due to the presence of salt in feed. The salt rejection was always more than 99.98 %.

4.3.3. The effect of SiO_2 NPs addition on the aggregate size

Fig. 4-8 summarises the possible mechanism for the change of the pore structure by the addition of SiO_2 NPs. When the concentration of SiO_2 NPs in the dope is as low as 1 %, the presence of SiO_2 NPs impedes the interaction between MWCNTs and PVDF, leading to the increase in the pore size at the surface (Fig. 4-8 above). When the SiO_2 NPs concentration is as high as 7 % the growth in macrovoids continues, leading to the disappearance of asymmetric structure (Fig. 4-8 below).

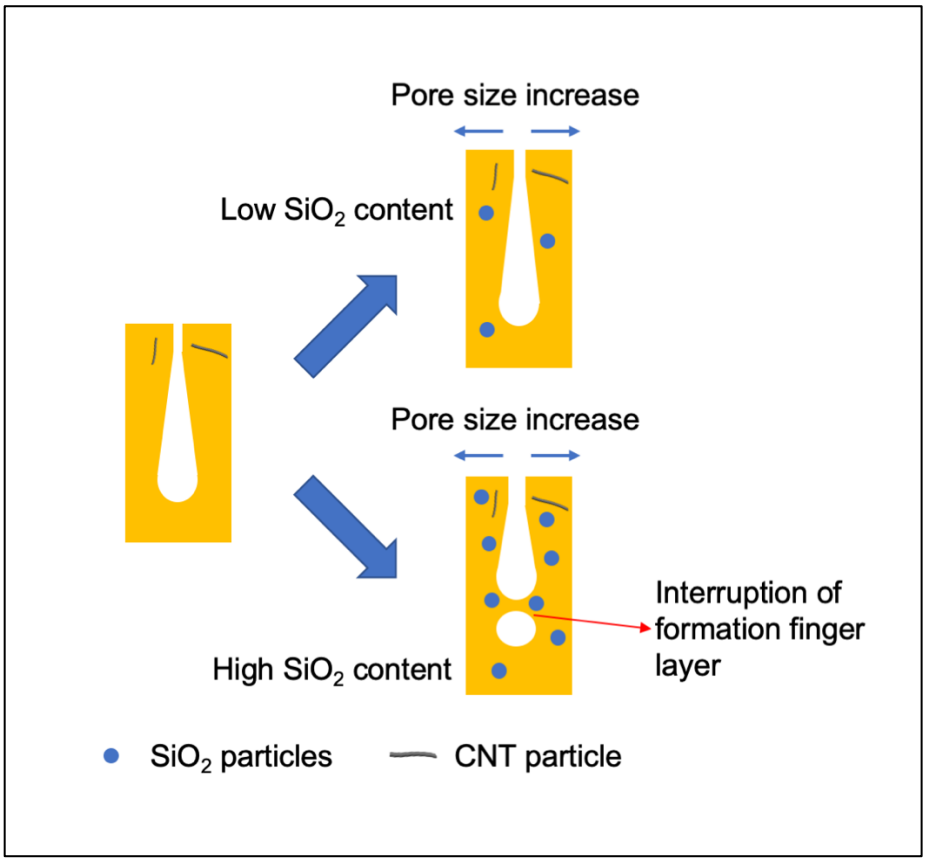

Fig. 4-8 Possible mechanism of change for membrane pores with introduction of SiO_2 NPs

The effect of SiO_2 NPs addition on the MWCNTs aggregation is in order. Pristine MWCNTs, with large surface area, easily aggregate in the polymer composite due to van der Waals force[24, 30-31]. The difficulties in dispersing MWCNTs has been considered as a major factor which retards the development of MWCNTs composites and their applications [30-31]. Even with high power ultrasonication, the MWCNTs are ready to aggregate in the membrane. The most common way to well-disperse MWCNTs into polymer composites is the functionalization of MWCNTs. It is proposed by this work that the addition of SiO_2 NPs is an alternative way to alleviate the aggregation of MWCNTs with the following evidences.

Fig. 4-9 shows the aggregate size distribution of MWCNTs obtained by the ImageJ analysis of the microscopic pictures. In the figure it is clearly shown that the aggregate size decreases with the increase in the concentration of S (superhydrophobic)-SiO_2. The other SiO_2 NPs also decrease the aggregate size, but the effect depends on the NPs' size, i.e. aggregate size is the smallest for B (hydrophobic, 15 nm), the largest for L (hydrophilic, 33 nm) and the intermediate for S (superhydrophobic, 20 nm). The possible reason for the decrease of the aggregate size may be that the introduction of SiO_2 NPs provides intensified shear forces to break the Van der Waal interaction between carbon atoms. The introduction of SiO_2 NPs may interact with carbon atom on the MWCNTs which impede the aggregation MWCNTs.

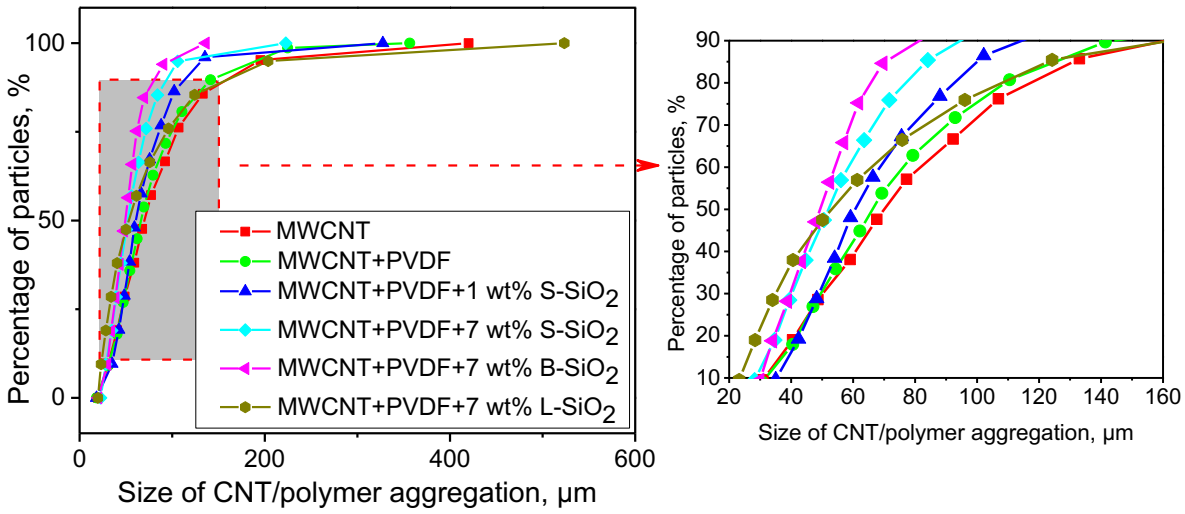

Fig. 4-9 Effect of SiO_2 NPs addition of the aggregate size distribution of CNTs.

Integrated nano-additives of MWCNTs and graphene into nanocomposites are known to improve electrical, thermal and mechanical properties of composites[21-23, 32-33]. The added MWCNTs could inhibit the aggregation of graphene nanoplates, leading to the improvement of their intrinsic properties as reinforced materials[34]. At the same time, the graphene nanoplates form a shield structure preventing MWCNTs damage during sonication[22]. The MWCNTs/SiO_2 NPs integrated nano-additives may be working by a different mechanism as SiO_2 NPs do not have plate-like structure. It should be noted, however, the improved dispersion of MWCNTs with SiO_2 NPs may or may not have a positive effect on the VMD performance because aggregation of MWCNTs has been suggested to improve the vapor flux through the membranes[13, 16].

The introduction of GO into the membrane could improve the fouling resistance, water permeability, selective and other performances of the membrane[35-39]. Inorganic integrated additives incorporated into the nanocomposite membranes have attracted much attention

as a promising way to improve the membrane performance in various membrane separation processes by enhancing nano-additives dispersion. As shown in Table 4-6 Graphene oxide (GO), with its unique structure, such as large surface area and number of reactive sites[40-44], as well as remarkable electrical and mechanical properties, was used as one of the additive components in most cases[35, 45]. Attempting further improvement of membrane performance, different inorganic nano-particles have been added to GO. Silicon dioxide (SiO_2) is one of common particles to be added to GO, showing improvement in performance[40, 43-44]. Similarly, Titanium dioxide (TiO_2) and GO integrated nano-additives was also proven to be effective [41-42, 46]. In order to improve the biofouling resistance for membrane, GO also has been decorated by silver and loaded onto the membrane surface[47].

Table. 4-6 Related studies about hybrid nano-additives on membrane

Reference	Integrated additives	Membrane type	Membrane application	Main effects on membrane
		Synthesize method		
40	GO/SiO_2	Polysulfone (PSf)	filtration	a. Improved antifouling capacity; b. improved hydrophobicity (Contact angle decrease) [a]
41, 46	GO/TiO_2	PVDF	ultrafiltration	
42	GO/TiO_2	PSf	ultrafiltration	
43-44	GO/SiO_2	PVDF	ultrafiltration	
47	GO/AgNPs	film composite membrane	Forward osmosis	
		Directly blending method		
24, 35, 48	GO/ MWCNT	PVDF	ultrafiltration	[b]
49	Two TiO_2	PVDF	Membrane distillation	Increased vapor permeation

[a] For all the ultrafiltration membrane, integrated additives could enhance water permeation through membrane.

[b] Blending method for GO/MWCNT additives has similar effects on membranes like synthesize method above.

It is obvious from Table 4-6 that this work stands out by its own uniqueness, i.e. there has been no work so far where the MWCNTs/SiO_2 NPs was used as integrated nano-additives, particularly for VMD.

4.4. Conclusions

The effect of adding integrated MWCNTs/SiO_2 nano-particles into PVDF nanocomposite membrane on the membrane's properties and VMD performance was investigated. At low SiO_2 NPs loading ratio to MWCNTs, the integrated additive exhibited a synergic effect on the VMD performance of the membrane. MWCNTs increase in overall porosity of the membrane (Chapter 3), while SiO_2 NPs increase the size of the macrovoids. As a result, the VMD flux with the salty feed increased 292 % and 55 %, respectively, from the pristine PVDF membrane and the MWCNTs blended membrane, even though LEPw slightly decreased and the tensile properties of the membrane were negatively affected.

When the SiO_2 loading ratio to MWCNTs was further increased the asymmetric structure of the membrane gradually disappeared, resulting in low porosities with compressed macrovoids. Thus, membranes of highest SiO_2 loading to MWCNTs (M-CN7), LEPw and the mechanical strength were too low despite their high VMD fluxes. Thus, M-C2L7 membrane with a VMD artificial salty water flux of 4.55 kg/(m^2·h), a very high salt

rejection of >99.98 % and improved LEPw, seems the best among the membranes prepared in this work.

Reference

1. Drioli, E.; Ali, A.; Macedonio, F., Membrane distillation: Recent developments and perspectives. Desalination 2015, 356, 56-84.
2. Abu-Zeid, M. A. E.-R.; Zhang, Y.; Dong, H.; Zhang, L.; Chen, H.-L.; Hou, L., A comprehensive review of vacuum membrane distillation technique. Desalination 2015, 356, 1-14.
3. González, D.; Amigo, J.; Suárez, F., Membrane distillation: Perspectives for sustainable and improved desalination. Renewable and Sustainable Energy Reviews 2017, 80, 238-259.
4. Baghbanzadeh, M.; Rana, D.; Lan, C. Q.; Matsuura, T., Effects of inorganic nano-additives on properties and performance of polymeric membranes in water treatment. Separation & Purification Reviews 2016, 45 (2), 141-167.
5. Eykens, L.; De Sitter, K.; Dotremont, C.; Pinoy, L.; Van der Bruggen, B., Membrane synthesis for membrane distillation: A review. Separation and Purification Technology 2017, 182, 36-51.
6. Hou, D.; Dai, G.; Fan, H.; Wang, J.; Zhao, C.; Huang, H., Effects of calcium carbonate nano-particles on the properties of PVDF/nonwoven fabric flat-sheet composite membranes for direct contact membrane distillation. Desalination 2014, 347, 25-33.

7. Efome, J. E.; Baghbanzadeh, M.; Rana, D.; Matsuura, T.; Lan, C. Q., Effects of superhydrophobic SiO_2 nanoparticles on the performance of PVDF flat sheet membranes for vacuum membrane distillation. Desalination 2015, 373, 47-57.
8. Silva, T. L.; Morales-Torres, S.; Figueiredo, J. L.; Silva, A. M., Multi-walled carbon nanotube/PVDF blended membranes with sponge-and finger-like pores for direct contact membrane distillation. Desalination 2015, 357, 233-245.
9. Baghbanzadeh, M.; Rana, D.; Lan, C. Q.; Matsuura, T., Effects of hydrophilic silica nanoparticles and backing material in improving the structure and performance of VMD PVDF membranes. Separation and Purification Technology 2016, 157, 60-71.
10. Ismail, A.; Goh, P.; Sanip, S.; Aziz, M., Transport and separation properties of carbon nanotube-mixed matrix membrane. Separation and Purification Technology 2009, 70 (1), 12-26.
11. Shawky, H. A.; Chae, S.-R.; Lin, S.; Wiesner, M. R., Synthesis and characterization of a carbon nanotube/polymer nanocomposite membrane for water treatment. Desalination 2011, 272 (1-3), 46-50.
12. Goh, P.; Ismail, A.; Ng, B., Carbon nanotubes for desalination: Performance evaluation and current hurdles. Desalination 2013, 308, 2-14.
13. An, A. K.; Lee, E.-J.; Guo, J.; Jeong, S.; Lee, J.-G.; Ghaffour, N., Enhanced vapor transport in membrane distillation via functionalized carbon nanotubes anchored into electrospun nanofibres. Scientific Reports 2017, 7, 41562.
14. Gethard, K.; Sae-Khow, O.; Mitra, S., Water desalination using carbon-nanotube-enhanced membrane distillation. ACS Applied Materials & Interfaces 2010, 3 (2), 110-114.

15. Dumée, L. F.; Sears, K.; Schütz, J.; Finn, N.; Huynh, C.; Hawkins, S.; Duke, M.; Gray, S., Characterization and evaluation of carbon nanotube Bucky-Paper membranes for direct contact membrane distillation. Journal of Membrane Science 2010, 351 (1-2), 36-43.
16. Tijing, L. D.; Woo, Y. C.; Shim, W.-G.; He, T.; Choi, J.-S.; Kim, S.-H.; Shon, H. K., Superhydrophobic nanofiber membrane containing carbon nanotubes for high-performance direct contact membrane distillation. Journal of Membrane Science 2016, 502, 158-170.
17. Yu, L.-Y.; Xu, Z.-L.; Shen, H.-M.; Yang, H., Preparation and characterization of PVDF–SiO_2 composite hollow fiber UF membrane by sol–gel method. Journal of Membrane Science 2009, 337 (1-2), 257-265.
18. Xiong, X.; Li, Q.; Zhang, X. C.; Wang, L.; Guo, Z. X.; Yu, J., Poly (vinylidene fluoride)/silica nanocomposite membranes by electrospinning. Journal of Applied Polymer Science 2013, 129 (3), 1089-1095.
19. Wang, X.; Wang, L.; Su, Q.; Zheng, J., Use of unmodified SiO_2 as nanofiller to improve mechanical properties of polymer-based nanocomposites. Composites Science and Technology 2013, 89, 52-60.
20. Khayet, M., Membranes and theoretical modeling of membrane distillation: A review. Advances in Colloid and Interface Science 2011, 164 (1-2), 56-88.
21. Li, J.; Wong, P.-S.; Kim, J.-K., Hybrid nanocomposites containing carbon nanotubes and graphite nanoplatelets. Materials Science and Engineering: A 2008, 483, 660-663.
22. Kumar, S.; Sun, L.; Caceres, S.; Li, B.; Wood, W.; Perugini, A.; Maguire, R.; Zhong, W., Dynamic synergy of graphitic nanoplatelets and multi-walled carbon nanotubes in polyetherimide nanocomposites. Nanotechnology 2010, 21 (10), 105702.

23. Chatterjee, S.; Nafezarefi, F.; Tai, N.; Schlagenhauf, L.; Nüesch, F.; Chu, B., Size and synergy effects of nanofiller hybrids including graphene nanoplatelets and carbon nanotubes in mechanical properties of epoxy composites. Carbon 2012, 50 (15), 5380-5386.
24. Zhang, J.; Xu, Z.; Shan, M.; Zhou, B.; Li, Y.; Li, B.; Niu, J.; Qian, X., Synergetic effects of oxidized carbon nanotubes and graphene oxide on fouling control and anti-fouling mechanism of polyvinylidene fluoride ultrafiltration membranes. Journal of Membrane Science 2013, 448, 81-92.
25. Chen, Z.; Rana, D.; Matsuura, T.; Yang, Y.; Lan, C. Q., Study on the structure and vacuum membrane distillation performance of PVDF composite membranes: I. Influence of blending. Separation and Purification Technology 2014, 133, 303-312.
26. Shi, L.; Wang, R.; Cao, Y.; Feng, C.; Liang, D. T.; Tay, J. H., Fabrication of poly (vinylidene fluoride-co-hexafluropropylene)(PVDF-HFP) asymmetric microporous hollow fiber membranes. Journal of Membrane Science 2007, 305 (1-2), 215-225.
27. Sukitpaneenit, P.; Chung, T.-S., Molecular elucidation of morphology and mechanical properties of PVDF hollow fiber membranes from aspects of phase inversion, crystallization and rheology. Journal of Membrane Science 2009, 340 (1-2), 192-205.
28. Lai, C. Y.; Groth, A.; Gray, S.; Duke, M., Enhanced abrasion resistant PVDF/nanoclay hollow fibre composite membranes for water treatment. Journal of Membrane Science 2014, 449, 146-157.
29. Baghbanzadeh, M.; Rana, D.; Matsuura, T.; Lan, C. Q., Effects of hydrophilic CuO nanoparticles on properties and performance of PVDF VMD membranes. Desalination 2015, 369, 75-84.

30. Ma, P.-C.; Siddiqui, N. A.; Marom, G.; Kim, J.-K., Dispersion and functionalization of carbon nanotubes for polymer-based nanocomposites: A review. Composites Part A: Applied Science and Manufacturing 2010, 41 (10), 1345-1367.
31. Das, R.; Ali, M. E.; Hamid, S. B. A.; Ramakrishna, S.; Chowdhury, Z. Z., Carbon nanotube membranes for water purification: A bright future in water desalination. Desalination 2014, 336, 97-109.
32. Yu, A.; Ramesh, P.; Sun, X.; Bekyarova, E.; Itkis, M. E.; Haddon, R. C., Enhanced thermal conductivity in a hybrid graphite nanoplatelet–carbon nanotube filler for epoxy composites. Advanced Materials 2008, 20 (24), 4740-4744.
33. Chatterjee, S.; Wang, J.; Kuo, W.; Tai, N.; Salzmann, C.; Li, W.; Hollertz, R.; Nüesch, F.; Chu, B., Mechanical reinforcement and thermal conductivity in expanded graphene nanoplatelets reinforced epoxy composites. Chemical Physics Letters 2012, 531, 6-10.
34. Yang, S.-Y.; Lin, W.-N.; Huang, Y.-L.; Tien, H.-W.; Wang, J.-Y.; Ma, C.-C. M.; Li, S.-M.; Wang, Y.-S., Synergetic effects of graphene platelets and carbon nanotubes on the mechanical and thermal properties of epoxy composites. Carbon 2011, 49 (3), 793-803.
35. Zhao, Y.; Xu, Z.; Shan, M.; Min, C.; Zhou, B.; Li, Y.; Li, B.; Liu, L.; Qian, X., Effect of graphite oxide and multi-walled carbon nanotubes on the microstructure and performance of PVDF membranes. Separation and Purification Technology 2013, 103, 78-83.
36. Zhao, H.; Wu, L.; Zhou, Z.; Zhang, L.; Chen, H., Improving the antifouling property of polysulfone ultrafiltration membrane by incorporation of isocyanate-treated graphene oxide. Physical Chemistry Chemical Physics 2013, 15 (23), 9084-9092.

37. Lee, J.; Chae, H.-R.; Won, Y. J.; Lee, K.; Lee, C.-H.; Lee, H. H.; Kim, I.-C.; Lee, J.-m., Graphene oxide nanoplatelets composite membrane with hydrophilic and antifouling properties for wastewater treatment. Journal of Membrane Science 2013, 448, 223-230.
38. Kumar, M.; McGlade, D.; Ulbricht, M.; Lawler, J., Quaternized polysulfone and graphene oxide nanosheet derived low fouling novel positively charged hybrid ultrafiltration membranes for protein separation. Rsc Advances 2015, 5 (63), 51208-51219.
39. Goh, K.; Setiawan, L.; Wei, L.; Si, R.; Fane, A. G.; Wang, R.; Chen, Y., Graphene oxide as effective selective barriers on a hollow fiber membrane for water treatment process. Journal of Membrane Science 2015, 474, 244-253.
40. Wu, H.; Tang, B.; Wu, P., Development of novel SiO2–GO nanohybrid/polysulfone membrane with enhanced performance. Journal of Membrane Science 2014, 451, 94-102.
41. Safarpour, M.; Khataee, A.; Vatanpour, V., Effect of reduced graphene oxide/TiO_2 nanocomposite with different molar ratios on the performance of PVDF ultrafiltration membranes. Separation and Purification Technology 2015, 140, 32-42.
42. Kumar, M.; Gholamvand, Z.; Morrissey, A.; Nolan, K.; Ulbricht, M.; Lawler, J., Preparation and characterization of low fouling novel hybrid ultrafiltration membranes based on the blends of GO− TiO_2 nanocomposite and polysulfone for humic acid removal. Journal of Membrane Science 2016, 506, 38-49.
43. Li, Z.-K.; Lang, W.-Z.; Miao, W.; Yan, X.; Guo, Y.-J., Preparation and properties of PVDF/SiO_2@GO nanohybrid membranes via thermally induced phase separation method. Journal of Membrane Science 2016, 511, 151-161.

44. Zhu, Z.; Jiang, J.; Wang, X.; Huo, X.; Xu, Y.; Li, Q.; Wang, L., Improving the hydrophilic and antifouling properties of polyvinylidene fluoride membrane by incorporation of novel nanohybrid GO@SiO_2 particles. Chemical Engineering Journal 2017, 314, 266-276.
45. Wang, N.; Ji, S.; Zhang, G.; Li, J.; Wang, L., Self-assembly of graphene oxide and polyelectrolyte complex nanohybrid membranes for nanofiltration and pervaporation. Chemical Engineering Journal 2012, 213, 318-329.
46. Safarpour, M.; Khataee, A.; Vatanpour, V., Preparation of a novel polyvinylidene fluoride (PVDF) ultrafiltration membrane modified with reduced graphene oxide/titanium dioxide (TiO_2) nanocomposite with enhanced hydrophilicity and antifouling properties. Industrial & Engineering Chemistry Research 2014, 53 (34), 13370-13382.
47. Soroush, A.; Ma, W.; Silvino, Y.; Rahaman, M. S., Surface modification of thin film composite forward osmosis membrane by silver-decorated graphene-oxide nanosheets. Environmental Science: Nano 2015, 2 (4), 395-405.
48. Zhang, J.; Xu, Z.; Mai, W.; Min, C.; Zhou, B.; Shan, M.; Li, Y.; Yang, C.; Wang, Z.; Qian, X., Improved hydrophilicity, permeability, antifouling and mechanical performance of PVDF composite ultrafiltration membranes tailored by oxidized low-dimensional carbon nanomaterials. Journal of Materials Chemistry A 2013, 1 (9), 3101-3111.
49. Li, Z.; Rana, D.; Wang, Z.; Matsuura, T.; Lan, C. Q., Synergic effects of hydrophilic and hydrophobic nanoparticles on performance of nanocomposite distillation membranes: An experimental and numerical study. Separation and Purification Technology 2018, 202, 45-58.

5. Conclusions

PVDF membranes blended with MWCNTs were fabricated by the phase inversion method in Chapter 3. With 2 wt. % MWCNTs loading, the maximum vacuum membrane distillation (VMD) performance was achieved, reaching 5.64 kg/(m^2·h) with distilled water feed and at 50 ºC. Comparing with pristine PVDF membrane, the vapor flux of this particular membrane increased 151%. The main reason for the improved VMD performance was the increase in porosity of the membrane. But the higher porosity at the same time caused the low LEPw and the weak tensile properties. Beside the increasing porosity, MWCNTs had significant impacts on the porous structure such as the reduction in surface pore size and elongation of finger-like pores.

In order to further improve the VMD flux, different SiO_2 NPs were integrated with CNTs as additives in chapter 4 which based on the result in Chapter 3. 2 wt. % MWCNTs concentration blended PVDF membrane was chose to further combine with SiO_2 different particles. Two SiO_2 concentrations in the dope were studied, one was 1 wt.% and the other 7 wt. %. When a smaller amount of SiO_2 (1 wt.%) was integrated with CNTs, further improvement in vapor flux was observed, i.e. the flux could reach 2.55 kg/(m^2·h) with 35 g/L sodium chloride solution as feed and at 30 ºC. Salt rejection higher than 99.97% could be maintained. This is due to a synergic effect of MWCNTs and SiO_2 NPs on the VMD flux. MWCNTs increase the overall porosity of the membrane, while SiO_2 NPs increase the size of the macrovoids. LEPw is lowered by the SiO_2 NPs addition.

With the addition of 7 wt. % SiO_2 NPs, the membrane showed the highest flux of 5.69 kg/(m^2·h) with distilled water feed and at 30 ºC. But the asymmetric structure of the membrane gradually disappeared, resulting in low porosities with compressed macrovoids. Thus, LEPw and the mechanical strength were too low despite their high VMD fluxes. Especially when the CNTs concentration was increased to 8 wt%, asymmetric structure of membrane completely disappeared. It was concluded from these results that the membrane performance is better improved by the integration of 1 wt.% SiO_2 with MWCNTs than the integration of 7 wt.% SiO_2.

In Chapter 4, it was also concluded that the SiO_2 NPs addition to CNTs reduces the size of CNTs aggregates. The larger the amount of SiO_2 NPs added the smaller the aggregate size.

Based on this study, it can be firmly concluded that blending of MWCNTs in PVDF with (different SiO_2 in Chapter 4) or without (only MWCNT in Chapter 3) integrating with other additives can improve the VMD flux. With relatively high production cost, CNTs blended membranes still could not compete with other mature MD membranes. In order to fully exploit the potential of CNTs as additives, functionalization of CNTs, fabrication methods other than nonsolvent induced phase inversion, integration of nano-additives other than SiO_2 NPs have to be thoroughly investigated.